ABSTRACT

Quantum Biophotonics: Applications to Plant Stress and Bacteria

Jeremy N. Kunz, Ph.D.

Mentor: Marlan O. Scully, Ph.D.

Drought stress disrupts the balance of macro- and micronutrients and affects the yield of agriculturally and economically significant plants. Rapid detection of stress-induced changes of relative content of elements such as sodium (Na), potassium (K), calcium (Ca) and iron (Fe) in the field may allow farmers and crop growers to counter the effects of plant stress and to increase their crop return. Unfortunately, the currently available analytical methods are time-consuming, expensive and involve elaborate sample preparation which hinders routine daily monitoring of crop health on a field scale. An alternative method for rapid detection of drought stress in plants using femtosecond laser-induced breakdown spectroscopy (LIBS) is proposed. Daily monitoring of relative contents of Na, K, Ca and Fe in decorative (gardenia) and cultivated outdoor (wheat) plant species under various degrees of drought stress is demonstrated. The observed differences in spectral and temporal responses indicate different mechanisms of drought resistance. Spectroscopic markers of drought stress which allow for distinguishing mild environmental and severe drought stress in wheat, may be used for remote field-scale estimation of plant stress and health.

Additionally, the ability to distinguish between crops and weeds using sensors from a distance will greatly benefit the farming community through improved and efficient scouting for weeds, reduced herbicide input costs and improved profitability. The utility of femtosecond LIBS for plant species differentiation is investigated. Greenhouse-grown plants of dallisgrass, wheat, soybean and bell pepper were evaluated using LIBS and elemental calcium transitions in plant tissue samples to measure plasma temperatures.

Finally, Ultraviolet radiation is an effective bacterial inactivation technique with broad applications in environmental disinfection. However, biomedical applications are limited due to the low selectivity, undesired inactivation of beneficial bacteria and damage of healthy tissue. Here, the effects of aluminum nanoparticles prepared by sonication of aluminum foil on the ultraviolet inactivation of *E. coli* bacteria are investigated and demonstrate a new radiation protection mechanism via plasmonic nano-shielding. Direct interaction of the bacterial cells with the aluminum nanoparticles and elucidate the nano-shielding mechanism via ultraviolet plasmonic resonance and nano-tailing effects are observed. The results provide a step towards developing improved radiation-based bacterial treatments.

Quantum Biophotonics: Applications in Plant Stress and Bacteria

by

Jeremy N. Kunz, B.S., M.A.

A Dissertation

Approved by the Department of Physics

_____

Dwight P. Russell, Ph.D., Interim Chairperson

Submitted to the Graduate Faculty of
Baylor University in Partial Fulfillment of the
Requirements for the Degree
of

Doctor of Philosophy

Approved by the Dissertation Committee

_____

Marlan O. Scully, Ph.D., Chairperson

_____

Howard Lee, Ph.D., Co-Chairperson

_____

Truell Hyde, Ph.D.

_____

Zhenrong Zhang, Ph.D.

_____

Johnathan Hu, Ph.D.

_____

Dmitri V. Voronine, Ph.D.

Accepted by the Graduate School

May 2017

_____

J. Larry Lyon, Ph.D., Dean

Page bearing signatures is kept on file in the Graduate School.

TABLE OF CONTENTS

LIST OF FIGURES

LIST OF TABLES

CHAPTER ONE

Introduction

Plants are affected by many types of biotic (insects, fungi, bacteria, viruses) and abiotic (salinity, drought, light, temperature) stress which can have a negative impact on agriculturally and economically significant florae [1, 2, 3, 4]. Global climate changes make the abiotic stress effects more adverse. It is important to understand complex physiological and molecular mechanisms of plant stress response in order to engineer stress tolerance and improve crop yield. The complex responses to stress in plants involve multiple steps including the signal perception by stress sensors, generation of signaling molecules such as reactive oxygen species (ROS) and abscisic acid (ABA), and modification of cellular ion contents of elements such as Ca, K, Na and Fe. The abiotic stress effects such as drought and salinity may be reduced by the timely application of relevant measures at the appropriate field locations. Therefore, early and rapid detection of various plant stresses has been the focus of extensive investigations.

Currently available technologies for detecting plant stress include plant tissue and soil water content monitors via thermography [5, 6], visible/near-infrared reflectance [7, 8], and UV-visible fluorescence imaging [9, 10, 11, 12]. These methods provide indirect information related to plant stress but do not directly measure the nutrient atomic and molecular concentrations. Other chemical analytical methods such as gas chromatography, mass spectrometry and nuclear magnetic resonance can provide such information on a laboratory scale but require time-consuming elaborate sample

preparation techniques. Rapid detection with little sample preparation is necessary to scale the sensing technology to the field size. LIBS provides the corresponding advantages and is therefore a promising candidate to address these challenges.

LIBS measurements are performed by focusing a laser pulse onto the sample surface causing ablation or vaporization of the sample material forming a plasma plume. The hot plasma breaks down the ablated material into elemental components, and excites electrons into higher energy levels. Once the hot plasma expands and cools, the electrons return to the ground state emitting photons of characteristic frequencies from atomic constituents [13]. Based on these spectroscopic signatures, LIBS has been used to differentiate between tissues [14], identify bacterial strains [15, 16], and determine soil pollution [17, 18]. LIBS has also been used for the analysis of the chemical composition of plants [19, 20, 21, 22, 23]. Semi-quantitative and quantitative measurements of Ca, K, Na, Fe, Mn, Zn, Pb, N and other elements were achieved in various plant species such as grasses, maize, wheat, clover, cotton, soy, spinach, sunflower, lettuce, potato, coffee, pepper, mango and many others. Here, the possibility of using LIBS for rapid detection of drought stress in wheat and gardenia is demonstrated by performing daily monitoring of relative concentrations of Ca, K, Na and Fe using LIBS and identified spectroscopic markers of mild and severe stress. These results may be extended to remote applications on the field scale using unmanned ground vehicle (UGV) and unmanned aerial vehicle (UAV) technologies. This technique developed here also has the potential to assist in the distinguishing and detection of stress induced by weed infestations of crops.

In agriculture, the ability to distinguish between crops and weed species from a distance using sensors has enormous practical applications. Growers and crop consultants

typically spend numerous hours each growing season scouting for the presence of weeds in production fields because effective weed management and crop yield protection relies on timely identification of weed issues and taking appropriate management decisions based on weed assessments [24]. Routine scouting for weeds serves as an important component of herbicide-resistance best management practices [25]. According to a recent report produced by the United States Department of Agriculture, scouting for weeds was the most widely practiced crop monitoring service in several crops [26]. Manual field scouting is not only an expensive and time-consuming process, but is inaccurate and often hampered by adverse weather conditions. Given the recent technological advancements in the arena of UGVs and UAVs, there is a possibility for carrying a suit of sensors and scout for weeds from above crop canopies at much higher precision and efficiency. While integration of various sensors with UGV/UAV platforms is continuing to evolve and payload limitations are being overcome, it is critical that targeted experiments are conducted under controlled environments to fully understand the capabilities and limitations of a diverse set of sensor tools for use in specific applications. For weed scouting applications, researchers have traditionally investigated tools such as GreenSeekers [27, 28], LIDAR [29, 30], Ultrasonic sensors [31, 32], DSLR cameras [33], multispectral cameras [34, 35] and, in some cases, hyperspectral sensors [36, 37].

The LIBS technology, widely employed in many industries for real-time monitoring of elemental and chemical composition [13, 38, 39], may have a great potential for use in plant species differentiation. Because LIBS is a simple but versatile modality, it has been applied in a host of analytical pursuits ranging from distinguishing between bacterial strains [40], analysis of meteorites and the Martian surface [41], and the

dating of archeological findings [41] to the classification of Chinese tea leaves [42], soil analysis [18, 41], and food science applications [43, 44, 45]. In particular, LIBS performs well in detecting minerals and metals, and is therefore an attractive technology for food process monitoring including: examining Ca in poultry processing [43], Pb and Si in wheat seedlings [44], and Na in baked goods [45]. LIBS has also been used in more fundamental capacities of food science in which nutrients and pesticides of raw agricultural products are examined [46]. During LIBS, the focused femtosecond laser pulses interact with the sample, vaporizing a small volume, and forming a plasma plume. The hot plasma breaks down the vaporized material into atomic components and excites electrons into higher energy states. As the plasma cools and expands, the electrons return to the ground state and emit photons at unique atomic frequencies [13].

Within the broad applications of LIBS, there is much flexibility in the performance of the technique. Pulses used for ablation of small amounts of sample surface can be obtained from nano-, pico-, and femtosecond lasers. Femtosecond pulses are of particular interest because high powers can be obtained with smaller energies; therefore, resulting in less damage to the sample [13]. Additionally, shorter pulse lengths allow for less interaction of the pulse with the formed plasma, causing a reduction in broad continuum background noise [13]. Femtosecond laser pulses have been used in plant science applications [19, 47, 48], medical purposes, such as in dentistry cavity preparation [49] and LASIK surgery [50, 51], and micromachining [52]. In particular, femtosecond laser pulses were found to yield more accurate results for applications where plant samples were employed due to the lower continuum background [47].

While there have been many studies using LIBS as a detection tool, an underutilized property of the technique is the use of the plasma temperature during ablation. The temperature of the plasma produced during LIBS depends on a number of factors, from pulse length and wavelength of the excitation laser to the angle of incidence and the composition of the sample [38]. During LIBS, a portion of the laser pulse energy is used to vaporize and ionize the sample. This required fraction depends on the molecular composition of the sample. After vaporization and ionization, the remaining portion of the laser pulse heats the plasma [39].

In the LIBS of plant matter, such as leaves, the plasma temperature will strongly depend on the molecular chemical composition. As most plants share common compounds; such as lignin [53] and cellulose [54], their different relative concentrations will result in a difference in the required energy to ionize the sample. Thus, the remaining pulse energy that heats the resultant plasma and excites the atomic and ionic transitions varies, and the measured peak ratios in the LIBS spectra characteristic of the plant species. The plasma temperature also depends on water concentration, as vacuole size affects the proportions of these compounds. Therefore, dried samples are preferred when measuring plasma temperature of different species in order to reduce the effects of water concentrations.

Several methods exist for the determination of the laser-induced plasma (LIP) temperature. Among the most common are the Boltzmann method, the Saha-Boltzmann method, the line-to-continuum method, and the synthetic spectra method [55]. The first two methods are quantum mechanical in nature and utilize the LIBS spectral line intensities in determining the LIP temperature; whereas, the line-to-continuum method is

semi-classical and exploits the continuum background in addition to the spectral line intensity [55]. The synthetic spectra method is mainly used to find the molecular temperature which is related to the heavy particle gas temperature [55]. In this work, the Boltzmann method was used to determine LIP temperature for different plants.

The aforementioned light-matter interactions have primarily been diagnostic or probing in nature. However, light has the potential to be employed so that as it interacts with material, the generated effects can be constrained to produce a desired outcome. One such possibility is to utilize light for the inactivation of harmful bacteria. Bacterial inactivation has recently received much attention due to the rising concern of antibiotic resistance [56]. Many alternative bacterial inactivation techniques have been developed such as photodynamic [57, 58, 59, 60] and photothermal [61, 62] treatments. Ultraviolet (UV) radiation has also been used for inactivating bacteria finding many applications such as the treatment of wound infections [63, 64], water [65, 66] and air [67, 68, 69] disinfection and many others.

UV radiation at 254 and 280 nm inactivates bacteria by damaging DNA and proteins, respectively [69, 70]. However, it does not discriminate between beneficial and pathogenic bacteria or healthy tissues. In order to develop selective bacterial UV disinfection treatments, it is necessary to improve UV protection techniques which could be used to counteract the UV inactivation for selected targets. The microparticle-based protection of fecal coliform bacteria in waste water was investigated [71]. In the former case, only a few types of bacteria have the ability to synthesize the Fe-based compounds. In the latter case, the disadvantage of the large size (> 20 μm) microparticles and low protection efficiency (< 1 %) limit the practical applications.

Here, the effects of aluminum nanoparticles (Al NPs) on the UV disinfection of *E. coli* bacteria and development of a new approach to protecting bacteria from the UV radiation using plasmonic nano-shielding are investigated.

Acknowledgements

The submitted manuscript entitled, "Rapid Detection of Drought Stress in Plants using Femtosecond Laser-Induced Breakdown Spectroscopy," has five contributing authors who are as follows: myself (Jeremy N. Kunz), Dmitri V. Voronine, Ho Wai Howard Lee, Alexei V. Sokolov, and Marlan O. Scully. Drs. Voronine, Sokolov, and Scully conceived and supervised the project. I built the experimental setup and performed all measurements with all data processing. Dr. Voronine and I analyzed the data and wrote the manuscript. Dr. Lee provided additional guidance as well as many useful discussions.

The published manuscript entitled, "Interaction of Femtosecond Laser Pulses with Plants: Towards Distinguishing Weeds and Crops using Plasma Temperature," has eight contributing authors and are as follows: myself, Dmitri, V. Voronine, Brian A. Ko, Ho Wai Howard Lee, Aman Rana, Muthukumar V. Bagavathiannan, Alexei V. Sokolov, and Marlan O. Scully. Dr. Dmitri and I conceived of the project and wrote the bulk of the manuscript. Drs. Voronine, Lee, Sokolov, and Scully supervised the project and provided guidance. Drs. Rana and Bagavathiannan provided plant samples, context for the project, and contributions to the introductory section of the manuscript. Brian A. Ko performed measurements. I performed data processing and analysis while Dr. Voronine assisted with data analysis.

The manuscript entitled, "Aluminum Plasmonic Nano-Shielding in Ultraviolet Inactivation of *E. coli* Bacteria," has seven contributing authors and are as follows: myself, Dmitri V. Voronine, Weigang Lu, Zachary Liege, Ho Wai Howard Lee, Zhenrong Zhang, and Marlan O. Scully. Dr. Voronine and I conceived of the project, performed data analysis, and wrote the manuscript. Dr. Lu provided Al nanoparticles. Zachary Liege performed SEM measurements. Drs. Voronine, Lee, Zhang, and Scully supervised the project. I performed all measurements, except for SEM measurements, grew *E. coli* bacteria samples, and performed SEM sample preparation.

CHAPTER TWO

Literature Review

In this chapter, I will review some of the many technological applications of light-matter interactions. Due to the depth and breadth of the subject, I will focus primarily on applications involving light and biological materials, or other industrial applications. Specifically, the chapter is subdivided into sections discussing applications of LIBS, current technologies for distinguishing between crops and weeds, and technologies pertaining to plasmonics and/or bacteria. A table summarizing the various LIBS techniques employed is included (see Table 2.1).

Laser-Induced Breakdown Spectroscopy

Hussain *et al*. applied nanosecond LIBS (4.5 μs gate delay) to samples of iron and steel slag samples [72]. Iron and steel slags are controlled by the environmental protection agency (EPA) which set limits to the concentration of certain elements that can be found within the slags. The authors found that many of their samples obtained from industry contain higher concentrations than allowable. For example, it was determined using LIBS that Cr concentration was 1866 ppm, while regulations allow for a maximum of only 1 ppm. LIBS was also used to quantify the purity level of open pit ore samples. Results were compared to the more accepted, yet sample preparation intensive, modality of ICP-OES and found to be in agreement.

Stelmaszczyk et al. sought to perform nanosecond LIBS on a target remotely [73]. Utilizing the Teramobile femtosecond laser system, the authors propagated the NIR laser

beam via filamentation to the stationary metal targets 90 m away. LIBS spectra were collected by a telescope system at the laser site. Due to the substantial distances between the LIBS system and the samples, no detection delay was required. Using the ultrashort pulsed laser to create filaments in the air, the authors were able to distinguish between copper and steel metal sample over a large distance. This technique can possibly be extended to kilometer distances as well.

In order to quantify the amount of Na and NaCl in baked goods, Bilge *et al*. used nanosecond LIBS with 0.5 μs gate delay and 20 μs gate width to monitor the Na 589 nm spectral line [45]. Comparing the LIBS technique to standard reference techniques, namely titration and atomic absorption spectroscopy, they found that the LIBS results were comparable and even more accurate when the sample being analyzed had artificial coloring. Additionally, the LIBS method was able to be conducted in under one minute and in real-time concluding that LIBS offers a viable option for monitoring of Na and NaCl content in bakery products even in the low salt limit.

Diaz *et al*. used LIBS to perform real-time evaluation the concentration of fertilizer, as well as selected macro- and micronutrients, in seven soil samples [18]. Gating delays and widths were varied from 0.1 to 5.3 μs in order to maximize the specific atomic spectrum to be analyzed. Limits of detection (LOD) and quantification (LOQ) were obtained and ranged from 4(22) ppm to 251(828) ppm LOD(LOQ) for Mg and P respectively; which are below typical elemental concentrations in soils. Results were heavily dependent on soil matrix composition and the authors propose using statistical analysis techniques in order to obtain better correlation between spectral intensities and total elemental concentrations.

LIBS was employed in an effort to determine heavy metal content in various types of soils. Capitelli *et al*. sampled several soils from around Europe of varying composition using nanosecond LIBS without gating [74]. Results were compared to the more standardized practice of inductively-coupled plasma (ICP) spectroscopy. The obtained spectra were successful in the qualitative determination of several heavy metals within the soils; however, was only able to yield semiquantitative results for heavy metal concentration. Therefore, more mature techniques such as ICP, which requires more intensive sample preparation than LIBS, yield quantitative concentrations.

Bousquet *et al*. also analyzed soil samples using nanosecond LIBS, without gating, along with Principal Components Analysis (PCA) [17]. By applying PCA to the entire LIBS spectrum, soil samples were able to be classified according to the concentrations of the major elements. This method exhibited the ability of LIBS to be used for quantitative analysis, unlike Capitelli *et al*. Measurements took place in a laboratory setting with a high resolution spectrometer (Aryelle, LTB). The authors also developed a mobile nanosecond LIBS instrument that uses a low resolution compact spectrometer (LIBS 2500, Ocean Optics) with hopes of performing similar analysis in the field.

Fang *et al*. sought to detect Hg as a signature for pollution in both soils and plant mater. Nanosecond LIBS, without delay, was employed [75]. Both soil and plant samples were compressed and pelletized and then doped with Hg contaminants. Initial results were unresolvable due to the presence of Fe in the samples which created overlap in the 253.65 nm Hg spectral line 253.68 nm Fe spectral line and by the presences of Bremstrahlung emission from the laser-induced plasma. Use of CCD detector and an

optical chopper allowed the 253.65 nm Hg spectral line to be resolved and concentrations of Hg pollutant in plant and soil samples to the 8 ppm detection level.

Trevizan *et al*. utilized nanosecond LIBS to analyze micronutrients (B, Cu, Fe, Mn, and Zn) in pelletized plant samples [76]. Gate delay and gate width were set to 2 μs. Limits of detection were found and ranged from 1.2 ppm to 3.0 ppm for Zn and B respectively. Concentration measurements were found to vary within a given sample from 4 to 30%. Results were also compared to ICP-OES and agreed reasonably well with a few exceptions. The authors propose various improvements to the sample preparation to increase reliability of LIBS findings.

Using nanosecond LIBS, with 1.2 μs gate delay and 4 μs gate width, Wang *et al*. successfully identified and distinguished six different types of tea leaves with 95.33% accuracy within testing samples [42]. This was done by comparing specific elemental lines (Mg, Mn, Ca, Al, Fe, K, CN, and C_2) found in each of the six types of tea leaves and using discriminant analysis methods. Dried, ground leaves were used to form compressed tablets for this study. This study demonstrated that LIBS can be successfully employed as a tool for categorizing of agricultural products.

Kim *et al*. utilized nanosecond LIBS in conjunction with a chemometric method (i.e. PLS-DA) to effectively detect and quantify nutrient elements (Mg, Ca, Na, and K) in spinach and rice and to distinguish pesticide-contaminated samples [46]. The LIBS results were found to be in good agreement with conventional inductively coupled plasma optical emission spectroscopy (ICP-OES) measurements of elemental concentration, but was performed much more rapidly. Dried, ground leaves were used to form compressed pellets for this study. These findings suggest that LIBS may be used as a tool for rapid

distinction of pesticide-contaminated agricultural products from pesticide-free agricultural products despite each having similar elemental compositions.

Bossu *et al*. utilized femtosecond LIBS, without delay or gating, to determine trace elemental pollutant deposition in sophora leaves from an urban environment [77]. The whole leaf was used without being ground and forming a pellet. Using this simplified technique, multiple trace elemental spectral lines were detected and compared for leaves of varying locations within the urban area. Bossu et al. propose that femtosecond LIBS may therefore be used as an instrument for real-time monitoring of atmospheric pollution, via absorption and deposition, in urban vegetation.

Arantes de Carvalho *et al*. compare femtosecond and nanosecond LIBS to quantify macro- (Ca, Mg, and P) and micronutrients (Cu, Fe, Mn, and Zn) in plant materials of different economically significant sample crops [47]. LIBS spectra were obtained with 35 ns gate delay and 250 ns gate width for femtosecond LIBS, and 0.75 μs gate delay with 3 μs gate width for nanosecond LIBS. Sample plant material were dried, ground, and pelletized for evaluation. It was found that femtosecond LIBS yielded nutrient concentration results in close agreement with ICP-OES verification and were less dependent on the chemical composition of the plant matrix; whereas, nanosecond LIBS can achieve similar accuracy only when coupled with more robust statistical methods.

Assion *et al*. look to compare spatial resolution for Ca^{2+} analysis in plant materials of femtosecond and nanosecond LIBS, each without gating. Strength of Ca^{2+} lines as compared to the plasma continuum background were observed for nanosecond and femtosecond LIBS of sunflower seedling stem [78]. It was found that the Ca2+ detection limit was comparable between the two techniques. However, the continuum

emission of the plasma was much smaller due to faster thermalization. Additionally, the threshold for the plasma generation was an order of magnitude less for the femtosecond laser pulse than the nanosecond pulse. Overall, it was observed that the femtosecond, rather than nanosecond, LIBS should be used for high spatial resolution demands on biological samples.

Samek *et al*. used femtosecond LIBS, without gating, to analyze the spatial distribution of Fe ions within plant materials [19]. Unlike other studies seeking to detect individual elements within plant matter, the authors utilized whole leaf samples for analysis. LIBS measurements were taken at the stem of the leaf samples and away from the stem. LIBS spectra reflect the spatial distribution of Fe ions expected from performing relaxation weighted magnetic resonance imaging (RWMRI) on the sample leafs. Results show higher concentrations of Fe in the stems, where it is transported within the leaf by the xylem, than in portions of the leaf between the veins.

Similarly, Galiova *et al*. used nanosecond LIBS (1 μs gate delay) to determine spatial distribution of Pb in hyperaccumulator plants, namely *Helianthus annuus* [79]. Pb distributions were determined in both the lateral (deep) and planar dimensions. Initial measurements were performed at the stem, where it was found to have the highest concentrations as expected, and subsequently at 500 μm steps in all directions along the plane of the leaf surface. Pb concentration mapping using LIBS was verified by X-ray microradiography and X-ray microtomography, and total concentrations determined by standard chemical analysis (without maintaining spatial information). LIBS has the potential to give both spatial information, as well as total concentration of Pb pollutants within plant materials.

Devey *et al*. performed nanosecond LIBS (1 μs delay) on pasture vegetation in order to measure elemental concentrations [23]. Pasture vegetation tested included perennial ryegrass (*Lolium perenne*) and white clover (*Trifolium repens*). Plant materials were oven dried, ground, and pelletized for testing. Several elements, including Na, K, Mg, Ca, and P were all measured by LIBS with a similar level of accuracy obtain from ICP-OES. However, other elements, namely Zn, Cu, and S, had uncertainties that were too high. The authors believe that LIBS can potentially replace ICP-OES as a less expensive and more productive method for measuring elemental concentrations found in pasture vegetation.

Kumar *et al*. used nanosecond LIBS to distinguish normal and malignant tumor cells in tissue [80]. They observed different elemental concentrations using LIBS and maximized the signal for each with by varying the gate delay time and gate width for each element. The LIBS results were compared to inductively coupled plasma emission spectroscopy (ICP-OES) measurements and were found to be in good agreement. From LIBS and ICPES data it was observed that that the concentration ratios of Ca, Cu, and Na with K are significantly different in normal tissue samples verses those with malignant cancer tissue samples.

Nanosecond and femtosecond LIBS have also been used to detect and identify other biological materials such as bacteria. Baudelet *et al*. used LIBS with 100 ns delay for each technique and 5 μs and 50 ns gate widths for femtosecond and nanosecond LIBS respectively [81]. It was observed that a spectral fingerprint was obtained for *E. coli* and *B. subtilis* bacteria that was used for detection and identification. Due to its lower plasma temperature and greater ratios between molecular and atomic emission lines (e.g. C_2/C,

CN/C), femtosecond LIBS was determined to be more favorable than nanosecond LIBS and provides a viable technology for discrimination between various bacteria or from the natural environment where they exist.

Samuels *et al*. performed nanosecond LIBS (1.5 μs delay) on a variety of biological material, including bacteria, molds, and spores [16]. The LIBS spectra were subsequently analyzed using principal-component analysis (PCA). The authors were able to successfully discriminate between the various biomaterials and with more rigorous analytical methods, the three bacteria tested, namely *B. thuringiensis*, *B. subtilis*, and *B. cereus*, could be distinguished as well. The authors believe that LIBS can be applied to test biological samples quickly to determine biological warfare threats.

Crops and Weeds

Using a femtosecond terawatt lidar system, Mejean *et al*. remotely probe air to detect and identify biological substances in air [82]. 800 nm wavelength femtosecond pulses were utilized to produce two-photon-excited fluorescence of a common fluorophore (riboflavin, 540 nm) contained in harmful bioagents (such as *B. anthracis*). The emitted fluorescence signal was collected remotely by a telescope and were distinguishable from the background water vapor. Effects could be observed up to 10 km away; however, the limiting factor is the phase control of the femtosecond pulse (demonstrated up to 100 m). This method demonstrates the need to develop technologies for long-range detection of biochemical and can possibly be extrapolated to detection of biochemical secreted by stressed plants in the field.

Table 2.1 Summary of LIBS applications

Author	Laser (wavelength)	Pulse length	Delay	Spectrometer	Sample
Arantes de Carvalho et al.	Ti:Sapphire (800 nm) Nd:YAG (1064, 532, 266 nm)	60 fs 6 ns	35 ns 0.75 µs	Shamrock 303i (Andor Technology)	Plant (pelletized)
Assion et al.	Ti:Sapphire(790 nm) Nd:YAG (355 nm)	30 fs 6 ns	- -	MS125 (Oriel)	Plant (whole leaf, fresh)
Baudelet et al.	Ti:Sapphire (810 nm) Nd:YAG (1064 nm)	120 fs 5 ns	100 ns 100 ns	Mechelle (Andor Technology)	Bacteria
Bilge et al.	Nd:YAG (532 nm)	-	0.5 µs	HR 2000 (Ocean Optics)	Bakery products
Bossu et al.	Ti:Sapphire (800 nm)	150 fs	-	-	Plant (whole leaf, fresh)
Bousquet et al.	Nd:YAG (1064 nm)	7 ns	-	LIBS 2500 (Ocean Optics)	Soil
Capitelli et al.	Nd:YAG (355 nm)	8 ns	-	(Andor Technology)	Soil
Devey et al.	Nd:YAG (1064 nm)	-	1 µs	-	Plant (pelletized)
Diaz et al.	Nd:YAG (1064 nm)	-	0.1-5.3 µs	SpectraPro 275 (Acton)	Soil
Fang et al.	Nd:YAG (1064 nm)	6 ns	-	Spex 1440	Soil/plant (pelletized)
Galiova et al.	Nd:YAG (532 nm)	5 ns	1 µs	TRIAX 320 (Jobin Yvon)	Plants (whole leaf, dried)
Hussain et al.	Nd:YAG (1064 nm)	8 ns	4.5 µs	LIBS 2000+ (Ocean Optics)	Slag, ore
Kim et al.	Nd:YAG (1064 nm)	7 ns	-	LIBS 2000+ (Ocean Optics)	Plant (pelletized)
Kumar et al.	Nd:YAG (532 nm)	5 ns	varied	ESA 3000 EV/I (LLA Instruments)	Malignant tissue
Samek et al.	Ti:Sappire (795 nm)	160 fs	-	ESA 3000 (LLA Instruments)	Plant (whole leaf, dried)
Samuels et al.	Nd:YAG (1064 nm)	10 ns	1.5 µs	LIBS 2000+ (Ocean Optics)	Bacteria, molds, spores
Stelmaszczyk et al.	Ti:Sapphire (800 nm)	800 fs	-	IS-SM 500 (Chromex)	Metal
Trevizan et al.	Nd:YAG (1064 nm)	5 ns	2, 5 µs	ESA 3000 (LLA Instruments)	Plant (pelletized)
Wang et al.	Nd:YAG (1064 nm)	6 ns	1.2 µs	SR-750-A (Andor Technology)	Plant (pelletized)

Lichtenthaler *et al*. employed a flash-lamp chlorophyll fluorescence imaging system to monitor the photosynthetic activity of an intact sample leaf in a non-invasive and rapid (few seconds) manner [10]. Illuminated the whole leaf with blue light from a Xenon flash lamp, the 690 nm fluorescence amplitude was recorded and imaged by a CCD camera. Water stress was able to be detected in a leaf that had been detached from the plant for only two hours and similar results were found in leaves that were still attached, but had been subjected to drought stress for ten days. This study demonstrated that under water stress, there is a detectable physiological change within the plant material and this method was effective at measuring this change.

In an effort to distinguish between crops and weeds from a great distance, Lamb *et al*. applied airborne multispectral imaging to map fields of a wheat and rye hybrid (*X Triticolsecale*, Wittmack) [35]. High-resolution images were obtained using a four-camera airborne video system. Each acquired image pixel was transformed into a normalized-difference vegetation index (NDVI) image and a soil-adjusted vegetation index (SAVI) image and compared. It was found that using 0.5 m spatial resolution, these methods were able to discriminate populations of weeds of 28 weeds m^{-2} and 17 weeds m^{-2} from weed free regions for NVDI and SAVI images respectively.

Gerhards *et al*. was able to perform real-time weed identification among several cereal crops using multispectral image analysis [34]. Two simultaneous images were taken of each plant, one in the red regime (550-570 nm) and one in the NIR region (770-1150 nm). Images were subtracted from each other and a contour of the plant was produced. This was transformed into a chain code and then into a function with a standardized contour length. This was compared to a database of 25 weeds and several

cereal crops. Computer-based decision making was used to determine amount of herbicide to apply for weed control when field sections with weed infestations levels were higher than the economic weed threshold. It was observed that in a space of four years, herbicide use went significantly down in all crops, but especially in winter cereals for grass-weed herbicides (90% reduction).

Lechoczky *et al*. applied hyperspectral imaging and LIDAR techniques to perform weed mapping [29]. Due to the significant impact that weeds have on agricultural outputs, accurate weed mapping is a very important part in precision agriculture. Using these two airborne techniques in conjunction, the authors were able to parse the observed patch of land into four categories, namely no vegetation, sparse, moderate and dense vegetation. Further improvements were suggested by the authors and include the use of higher resolution terrestrial LIDAR scanners.

Goel *et al*. sought to remotely determine the nitrogen content of corn (*Zea mays*) crops as well as to distinguish the corn from invasive weeds [37]. With a spatial resolution of 2 m, hyperspectral reflectance observations in 72 wavebands in the visible and NIR regime (408.73 to 947.07 nm) via a compact airborne spectrographic imager (CASI). By observing the spectral response curves, in particular the amplitude of the peak centered at 550 nm and the intensity of the NIR region and statistical analysis, regions of varying nitrogen content and weed populations among the corn crops.

Chaerle *et al*. inoculated tobacco leaves with tobacco mosaic virus (TMV) and monitored the disease with the leaves both visually and in the IR regime (8 to 12 μm) [5]. As the TMV disease takes hold within the leaf, salicylic acid (SA) is produced by the plant as a signal in defense against the pathogen. The production of SA within the plant

leaf causes a rise in local temperature within the leaf. As the inoculated tobacco leaves were observed, it was found that the local heating effects of the SA production was visualized with the high resolution IR camera. These thermal lesions were able to be detected 8 hours before the initial visual appearance of the necrotic tissue within the tobacco leaf. The ability to detect disease in the presymptomatic state could potentially allow farmers and crop growers to treat diseased crops earlier that currently available to increase crop yield.

Carter, on the other hand, measured spectral reflectance in the visible and IR regimes to determine plant stress for different stress agents and plant species [83]. Reflectance measurements were made in the laboratory setting using a scanning spectroradiometer over 768 calibrated channels. It was observed that visible reflectance increased reliably irrespective of stress type and plant species particularly in the regions of 491-575 nm and 647-760 nm. Other specific changes were also observed for specific stresses and species. Changes in IR spectral reflectance were observed only for drought stressed plants and when other stress had developed adequately to cause serious leaf dehydration as the reduction in water altered the sensitivity near the water absorption bands (1.45, 1.94, and 2.50 μm). This method may afford improved proficiency at detecting plant stress at whole plant and vegetated landscape level.

Penuelas *et al*. utilize both visible and NIR reflectance techniques for identifying plant physiological status [7]. Chlorophyll concentrations can be determined using visible wavelengths (e.g. 550 and 675 nm) which can be used to monitor photosynthetic activity. Water content within plants can be ascertained by reflectance spectra in the 1300-2500 nm and 950-970 nm ranges for individual leaves and whole plants/canopies respectively.

Chlorophyll and water content can be used in determining plant chemical composition and biomass, and accordingly plant physiological status.

Plasmonics/Bacteria

Using a normal LED (660 nm), Simon *et al*. was able to perform photodynamic therapy (PDT) on human lung carcinoma [84]. Modifications to traditional Au nanoparticles (20 nm diameter) were made by adding methylene blue (MB) to the surface. The MB-loaded Au nanoparticles increased the probability of singlet oxygen production over the typical therapy of MB photosensitized alone. Also, the addition of the Au nanoparticles to the MB was found to protect the important photosensitizer from enzymatic reduction; therefore, improving the overall effectiveness of the PDT. Overall, it was found that performing PDT with an ordinary LED and MB loaded Au nanoparticles was able to reduce cell viability down to a mere 13%.

Idris *et al*. used a similar approach by adding photosensitizers to mesoporous-silica-coated upconversion fluorescent nanoparticles (UCNs) [85]. The UCNs emit two main peaks at 540 and 660 nm when irradiated with 980 nm light. The photosensitizers used have high absorption cross-sections at these peak wavelengths. This study was performed both *in vitro* and *in vivo*. The authors found multiple benefits from using this approach. First, by using wavelengths in the NIR regime, it was found that larger penetrations depths were achieved over photons in visible frequencies. Second, the use of the dual photosensitizing agents produced enhanced therapeutic efficacy.

Bhana *et al*. combined Au nanorods with silicon 2,3-naphthalocyanine dihydroxide (SiNC) to form a sub-100 nm nanosystem for coinciding photothermal (PTT) and photodynamic therapies [86]. Au nanorods were grown to an aspect ratio of

approximately 4:1 (50 nm height, 12 nm diameter) with a plasmonic resonance at 800 nm. SiNC was loaded on to the Au nanoroads via electrostatic adsorption. Synthesized nanosystems were combined with head and neck cancer cells and irradiated at 808 nm by a laser diode for 10 minutes. The authors report that the combined PDT and PTT of the cancerous cells led to the improvement of cell death over a single therapy of either PDT or PTT alone.

Ayala-Orozco *et al*. have shown that the type of nanoparticle used for photothermal ablation of cancer cells can make a difference in outcome [87]. Using Au nanomatryoshkas verses Au nanoshells, they found that the nanomatryoshkas particles exhibit higher thermal transduction efficiency over the standard Au nanoshells due to their large absorption cross section. These Au nanomatryoshka particles were coupled with a NIR laser for a single treatment to tumor-bearing mice and were found to be disease free over 60 days later at a higher percentage than Au nanoshell and NIR laser treatment in tumor-bearing mice.

Santos *et al*. utilized 785 nm NIR laser in conjunction with novel nanoporous gold disk (NPGD) arrays to inactivate samples of *E. coli*, *B. subtilis*, and *Exiguobacterium* [62]. Measurements made using an infrared thermographic camera showed that local temperatures within the NPGD arrays upon excitation by the NIR laser were found to be about 200ºC with a temperature elevation rate of 26ºC/s for the first three seconds of irradiation. Since *E. coli* is more susceptible to thermal effects, it was found that 100% of *E.* coli cells were inactivated after only 5 s of irradiation with the NPGDs; whereas, the *B. subtilis* and *Exiguobacterium* samples required 25 s of irradiation for 100% cell inactivation. This technique provides for rapid *in vivo* inactivation of bacteria.

Zharov *et al*. developed a novel approach to the photothermal inactivation of bacterial samples [61]. *S. aureus* bacteria were combined with Au nanoparticles of various diameters (10, 20, and 40 nm). The Au nanoparticles were selectively bound to the surface of the *S. aureus* cell membrane by utilizing a monoclonal antibody. Once bound, the samples were illuminated with the second harmonic (532 nm) of a Q-switch Nd:YAG laser for 100 pulses. Samples of *S. aureus* bacteria without any Au nanoparticles showed no response to the laser irradiation. Whereas, all samples containing Au nanoparticles inactivated some bacteria with 10 nm diameter Au nanoparticles being the least effective and 40 nm diameter Au nanoparticles being the most effective; with approximately 20% cell inactivation and 90% cell inactivation respectively.

Dai *et al*. used a simple LED with emission centered at 415 nm to treat full-thickness burns infected with opportunistic *P. aeruginosa* bacteria in mice [63]. Their results show that the wavelength used left the normal tissue, and specifically the keratinocytes, unaffected while significantly damaging and killing the *P. aeruginosa* bacteria. After a single dose of blue light to the infected burn, 100% of mice treated survived, whereas, only 18.2% of untreated mice survived with the majority dying after just three days after inoculation. It was found that the damage done to the *P. aeruginosa* was associated with the intracellular chromophores excited by the blue light.

El-Azizi *et al*. sought to assess the effectiveness of low-dose UVC (254 nm) light in combination with antibiotics to disinfect catheter biofilms [88]. Vascular catheters were placed into a novel device, developed by the authors, allowing the inner lumen and outer surface of the catheters to be exposed to bacteria and allowed biofilm formation.

Biofilm forming bacteria assayed included methicillin-susceptible *S. aureus* (MSSA), methicillin-resistant *S. aureus* (MRSA) and *S. epidermidis*. Once biofilms were formed, catheters were removed and irradiated by a mercury lamp with an irradiance of 6.4 mW/cm^2 a distance of 10 cm from the lamp for five minutes. Samples were then treated with an antistaphylococcal antibiotic such as vancomycin, quinupristin/dalfopristin, or linezolid at double the minimum bactericidal concetrations. Bacterial cell inactivation was then assessed after 24 hours incubation to determine the efficacy of the treatment. It was observed that treatment alone of either UVC or an antistaphylococcal antibiotic was effective at inactivating the bacterial biofilms. However, the combine treatment of UVC and antisaphylococcal antibiotics significantly reduced the number of viable cells, but did not eradicate them completely.

Using a prototype LED which emits in the UVC regime (265 nm), Dean *et al*. analyzed the effectiveness of UVC light for the treatment of corneal bacterial infections. Samples of *S. aureus*, *E. coli*, *P. aeruginosa*, and *S. pyogenes* were plated and irradiated with the UVC LED (1.9 and 57.95 mJ/cm^2 fluence) from 1 to 30 seconds [89]. It was discovered that 100% of inhibition of growth was achieved for all bacterial varieties tested for 1 s of exposure time at 1.9 mJ/cm^2 fluence. Using the same UVC LED, human corneal epithelial cells were placed on a glass coverslip and irradiated for the same times and fluences. After the longest exposure time (30 s), there was no significant decrease in the ratio of live to dead cells as compared to the control samples.

Madge *et al*. evaluated the effectiveness of UVC (253.7 nm) light in disinfecting fecal coliform in wastewater [71]. Wastewater samples were separated into categories determined by the size of particulates within the wastewater. It was observed that

different sizes of particles in the wastewater correlated with the bacterial concentrations of the samples. Particulate size had direct effects on disinfection rates with samples containing larger fractions exhibiting slower disinfection rates and increased tailing within the data sets.

CHAPTER THREE

Rapid Detection of Drought Stress in Plants Using Femtosecond Laser-Induced Breakdown Spectroscopy

Abstract

Drought stress disrupts the balance of macro- and micronutrients and affects the yield of agriculturally and economically significant plants. Rapid detection of stress-induced changes of relative content of elements such as sodium (Na), potassium (K), calcium (Ca) and iron (Fe) in the field may allow farmers and crop growers to counter the effects of plant stress and to increase their crop return. Unfortunately, the currently available analytical methods are time-consuming, expensive and involve elaborate sample preparation such as acid digestion which hinders routine daily monitoring of crop health on a field scale. We report application of an alternative method for rapid detection of drought stress in plants using femtosecond laser-induced breakdown spectroscopy (LIBS). We demonstrate daily monitoring of relative content of Na, K, Ca and Fe in decorative indoor (gardenia) and cultivated outdoor (wheat) plant species under various degrees of drought stress. The observed differences in spectral and temporal responses indicate different mechanisms of drought resistance. We identify spectroscopic markers of drought stress which allow for distinguishing mild environmental and severe drought stress in wheat and may be used for remote field-scale estimation of plant stress resistance and health

Introduction

Plants are affected by many types of biotic (insects, fungi, bacteria, viruses) and abiotic (salinity, drought, light, temperature) stress which can have a negative impact on agriculturally and economically significant florae [1-4]. Global climate changes make the abiotic stress effects more adverse. It is important to understand complex physiological and molecular mechanisms of plant stress response in order to engineer stress tolerance and improve crop yield. The complex responses to stress in plants involve multiple steps including the signal perception by stress sensors, generation of signaling molecules such as reactive oxygen species and abscisic acid, and modification of cellular ion contents of elements such as Ca, K, Na and Fe. The abiotic stress effects such as drought and salinity may be reduced by the timely application of relevant measures at the appropriate field locations. Therefore, early and rapid detection of various plant stresses has been the focus of extensive investigations

Currently available technologies for detecting plant stress include plant tissue and soil water content monitors via thermography [5,6], visible/near-infrared reflectance [7,8], and UV-visible fluorescence imaging [9-12]. These methods provide indirect information related to plant stress but do not directly measure the nutrient atomic and molecular contents. Other chemical analytical methods such as gas chromatography, mass spectrometry and nuclear magnetic resonance can provide such information on a laboratory scale but require time-consuming elaborate sample preparation techniques. Rapid detection with little sample preparation is necessary to scale the sensing technology to the field size. LIBS provides the corresponding advantages and is therefore a promising candidate to address these challenges.

LIBS measurements are performed by focusing a laser pulse onto the sample surface causing ablation or vaporization of the sample material forming a plasma plume. The hot plasma breaks down the ablated material into elemental components, and excites electrons into higher energy levels. Once the hot plasma expands and cools, the electrons return to the ground state emitting photons of characteristic frequencies from atomic constituents [13]. Based on these spectroscopic signatures, LIBS has been used to differentiate between tissues [14], identify bacterial strains [15,16], and determine soil pollution [17,18]. LIBS has also been used for the analysis of the chemical composition of plants [19-23]. Semi-quantitative and quantitative measurements of Ca, K, Na, Fe, Mn, Zn, Pb, N and other elements were achieved in various plant species such as grasses, maize, wheat, clover, cotton, soy, spinach, sunflower, lettuce, potato, coffee, pepper, mango and many others.

Within the broad applications of LIBS, there is much flexibility in the performance of the technique. Pulses used for ablation of small amounts of sample surface can be obtained from nano-, pico-, and femtosecond lasers. Femtosecond pulses are of particular interest because high powers can be obtained with smaller energies; therefore, resulting in less damage to the sample [13]. Additionally, shorter pulse lengths allow for less interaction of the pulse with the formed plasma, causing a reduction in broad continuum background noise [13]. Femtosecond laser pulses have been used in plant science applications [19,21,24], medical purposes, such as in dentistry cavity preparation [25] and LASIK surgery [26,27], and micromachining [28]. In particular, femtosecond laser pulses were found to yield more accurate results for applications where plant samples were employed due to the lower continuum background [24]. Here, we

demonstrate the possibility of using LIBS for rapid detection of drought stress in wheat and gardenia. We performed daily monitoring of relative contents of Ca, K, Na and Fe using LIBS and identified spectroscopic markers of mild and severe stress. Our results may be readily extended to remote applications on the field scale using unmanned ground vehicle (UGV) and unmanned aerial vehicle (UAV) technologies.

Results

Drought stress in decorative and crop plants

We performed LIBS measurements on decorative indoor and cultivated outdoor plants such as gardenia and wheat, respectively. Gardenia plants are fragrant flowering evergreen shrubs or trees typically used as decorative plants. Wheat is a major cereal crop ranked third in the U.S. in overall farm revenues, and drought stress has been shown to cause substantial reduction in wheat crop yield [29]. We induced drought stress conditions by withdrawing water in these two plant species and measured the effects on watered (non-stressed) and non-watered (stressed) samples. The details of sample preparation and stress measurements are described in the Methods section. Figure 1(a) shows visual signatures of drought stress in gardenia which are revealed as wilting and color change in the non-watered (stressed) plant on day 31. The corresponding relative water content in % of day 0 is shown in Fig. 1(b). The water content stayed constant in the watered (non-stressed) plant and gradually decreased in the stressed plant. Similar results were obtained for wheat [Figs. 1(c) and 1(d)]. The constancy of the relative water content of the watered (non-stressed) sample plants pertains to the stability of the system. However, the visual signatures of stress were observed in both watered and non-watered

wheat plants. The stress effects on the watered wheat were attributed to the indoor lighting conditions imposed during the LIBS measurements for the entire treatment period. Visual inspection could not clearly distinguish between these mild environmental lighting (mild stress) effects from the drought (severe stress). We were able to distinguish these types of stress using LIBS as described below.

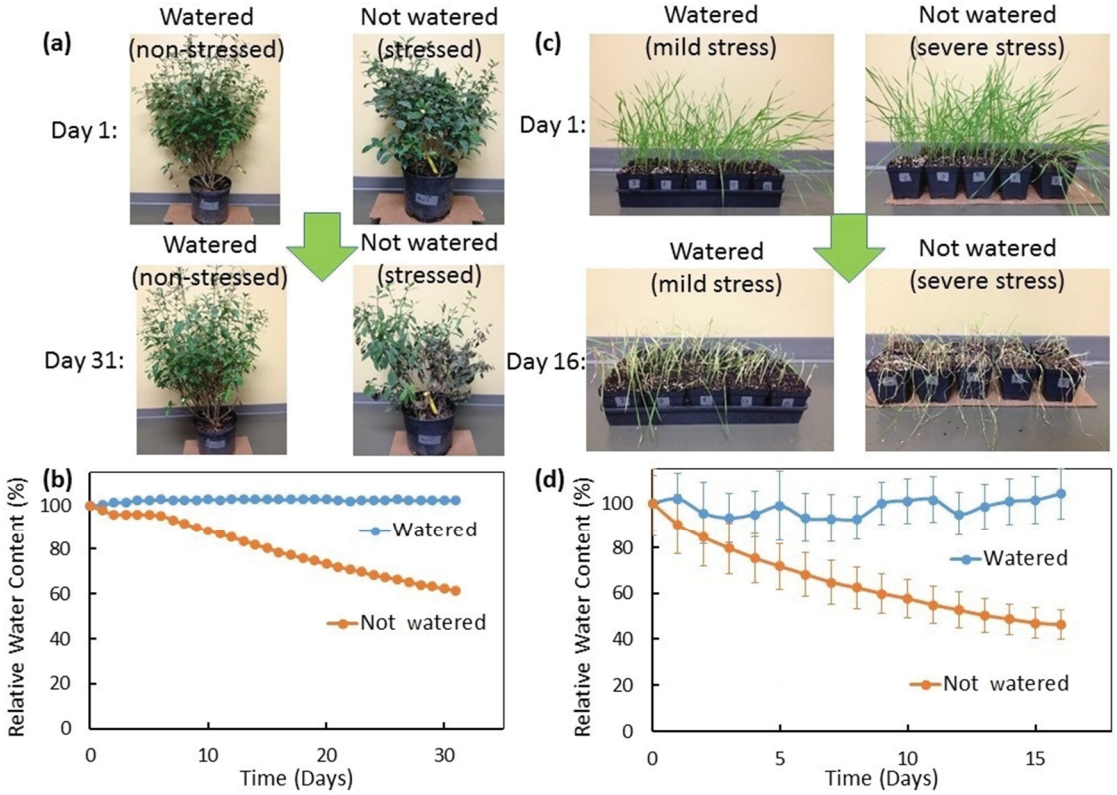

Figure 3.1. Visual signatures of drought stress and water content. Photographs of gardenia (a) and wheat (c) plants on the first and last days of the treatment periods for both watered and stressed non-watered treatment groups. Corresponding plots showing relative water content (% of day 0) for gardenia (b) and wheat (d) plants for the entire treatment periods.

Atomic spectral signatures of plant stress

The schematic of LIBS measurements of plant stress is shown in Figs. 2(a) and 2(b) for the non-stressed and stressed plants, respectively. The high intensity beams of

femtosecond laser pulses were focused on leaf samples placed on the translation stage that was scanned during the spectral measurements to replace the ablated areas for consecutive data points. We observed significant changes in the LIBS spectra taken from the stressed versus non-stressed plants over a time span of approximately one month for gardenia and two weeks for wheat plants [Fig. 2]. The LIBS spectra consisted of a set of narrowband peaks on top of a broadband background. The observed peaks were compared to the previous work [29-33] and assigned according to the NIST atomic spectral line database [34] based on the macro and micronutrients acquired by plants from the soil and air [35] [Figs. 2(c) and 2(h)]. We identified Na, Ca, O and Fe in gardenia [Fig. 2(c)] and Na, K, Ca, O and Fe in wheat [Fig. 2(h)]. The K peak was absent in gardenia [Figs. 2(d) and 2(f)] and in the non-stressed [Figs. 2(i) and 2(k), black lines] and mildly stressed [Fig. 2(i), red line] wheat. However, it was clearly identified in the severely stressed wheat [Fig. 2(k), red line] and therefore can be used as a spectroscopic marker for the detection of drought stress. Similarly, the Fe peaks were absent in the non-stressed gardenia [Figs. 2(d), red and black lines, and 2(f), black line] and wheat [Figs. 2(i) and 2(k), black lines] plants, but were present in the stressed gardenia [Fig. 2(f), red line] and wheat [Figs. 2(i) and 2(k), red lines]. The observed wavelengths for each designated peak from Fig. 2 can be found in Table 1.

Table 3.1 Peak assignments of the observed LIBS signals based on the NIST atomic spectral database [34].

Observed Peak (nm):		Element (NIST wavelength in nm):
Gardenia:	Wheat:	
383	383	Fe I (383.92556)
393	393	Ca II (393.366)
397	397	Ca II (396.847)
-	405	K I (404.7208)
423	423	Ca I (422.673)
431	431	O II (430.8999)
446	446	Na II (445.5224)
519	519	Ca I (518.885)
560	560	Ca I (559.849)
589	590	Na I (588.9950954)

Na peaks were observed in all LIBS spectra. The Na peak intensities varied depending on the presence and degree of stress. Figure 2(e) shows no significant change in the intensity of the Na peak in the control case of the non-stressed gardenia. However, the corresponding Na peak intensity significantly increased in the stressed gardenia plant [Fig. 2(g)]. Similar changes were also observed for the mildly and severely stressed wheat as shown in Figs. 2(j) and 2(l), respectively. Larger peak intensity difference was obsesrved for the Na peak of the severely stressed compared to the mildly stressed wheat. These results indicate that the relative change of the Na peak intensity can be used as a spectroscopic marker of plant stress.

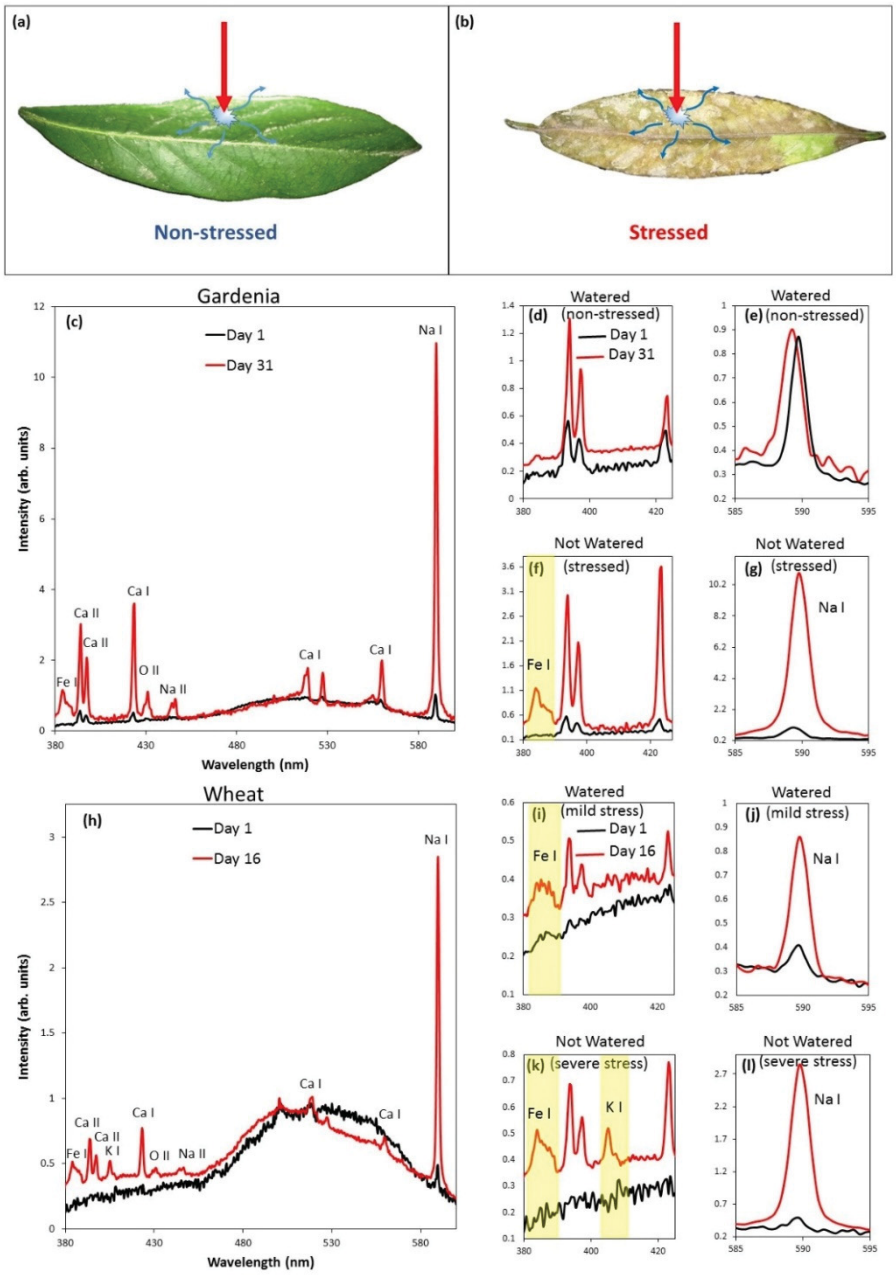

Figure 3.2. Atomic spectral signatures of abiotic stress in gardenia and wheat. Schematic of the LIBS experiment on a non-stressed (a) and stressed (b) plant. A high intensity beam of femtosecond laser pulses is focused onto the surface of a plant leaf generating emission of light from atomic components of laser-induced hot plasma. LIBS spectra of gardenia (c) – (g) and wheat (h) – (l) plants: (c) and (h) show LIBS signals collected in the selected full spectral range on the last day of the treatment for the stressed plants; spectral regions of interest show relative changes in the LIBS signals of watered (d, e, I, j) and non-watered (f, g, k, l) plants on the first (black line) and last (red line) days of treatments. Peak assignments of major LIBS signals are shown in (c) and (h). Na, K and Fe peaks which are used for detection of plant stress are highlighted. The shown spectra are averages of twenty LIBS spectra from each sample.

Ca peak intensities also varied as a response to stress in gardenia. No Ca peaks were detected in the LIBS spectra of the non-stressed wheat [Figs. 2(i) and 2(k), black lines]. Therefore, Ca peaks can also be used as spectral signatures of plant stress. However, similar Ca peaks were observed due to both mild [Fig. 2(i), red line] and severe [Fig. 2(k), red line] stress. Therefore, Ca cannot be used to distinguish between these different stresses. Figure 2 shows qualitative results of plant stress detection. Semi-quantitative information may be obtained from the analysis of peak ratios as described below.

Temporal response to drought stress

We investigated the temporal response of gardenia and wheat plants to drought stress by analyzing the daily evolution of LIBS signals. Although slight signal fluctuations were observed in all LIBS peaks for the non-stressed plants, the most significant changes were observed for the stressed samples. We established three different approaches for the plant stress detection using LIBS by monitoring the temporal evolution of nutrient LIBS signals, plasma temperatures and relative nutrient contents. Figure 3 shows the temporal evolution of the normalized average peak intensities for the selected Na, Ca and Fe elements observed in the LIBS spectra of gardenia and wheat. The effects of the drought stress in the LIBS spectra became more significant at the end of the treatment periods. In order to quantify the degree of these changes Fig. 3(a) shows the root-mean-square (rms) values of the difference between the average signal intensities of the stressed and not-stressed samples. This analysis shows that the 589 nm Na I peak had the greatest change over the course of the treatment. Temporal evolution plots of Na, Ca and Fe show that the major changes in nutrient LIBS signals happened during the last

two and five days of the treatment periods for the gardenia and wheat, respectively. The two gardenia sets with one plant per treatment group showed similar behavior.

As a second approach of plant stress detection, the plasma temperatures were calculated using Ca I signals for each day of the treatment period. Figure 3(b) shows rms values of the difference in plasma temperature between the stressed and non-stressed samples. The plasma temperatures remained constant until the last day of the treatment cycle for gardenia and randomly fluctuated during the last five days for wheat. This suggests that the plasma temperature may be used as another indicator of plant stress. However, care must be taken in more precise semi-quantitative use due to the lack of correlation between the plasma temperature and the stress-induced changes of nutrient LIBS signals. To obtain semi-quantitative information about the changes in relative nutrient contents we analyzed the LIBS peak ratios.

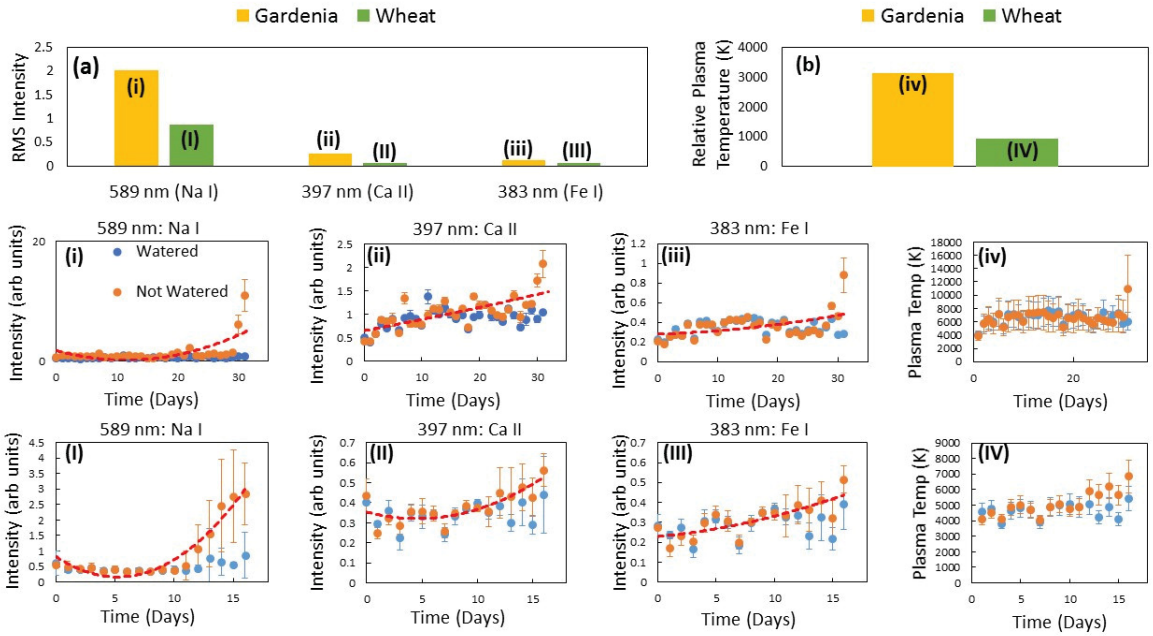

Figure 3.3. Temporal evolution of nutrient LIBS signals and plasma temperature. (a) Difference in average peak intensities (rms) between watered and non-watered plants for the selected Na, Ca and Fe elements observed in the LIBS spectra of gardenia (yellow bars) and wheat (green bars) plants. (b) Difference in average plasma temperatures (rms) between watered and non-watered plants. Temporal evolution of nutrient LIBS signals and plasma temperatures for the watered (blue circles) and non-watered (orange circles) gardenia (i) – (iv) and wheat (I) – (IV) plants during the entire treatment periods.

Temporal evolution of relative nutrient contents were obtained by taking the ratios of the nutrient LIBS signals and plotted over the entire treatment periods [Fig. 4]. Significant changes in the relative nutrient contents are clearly seen during the last five days of the treatment periods for both gardenia and wheat plants in Figs. 4(i) – 4(iv) and Figs. 4(I) – 4(IV), respectively. By comparison, the absolute values of the nutrient LIBS signals showed significant changes only for the last two days for gardenia. This demonstrates the advantage of using peak ratios for more precise detection of plant stress. Two Ca peaks were chosen as a control to insure the accurate measurement of the relative contents [Figs. 4(iv) and 4(IV)]. Rms values of the difference in peak ratios between the

watered and non-watered plants for the selected Na, Ca and Fe peaks are shown for gardenia (yellow bars) and wheat (green bars) in Fig. 4(a). The peak ratios which involve Na show a large difference between the watered and non-watered samples. Conversely, the ratio between two Ca peaks shows a negligible difference. Additionally, the ratio between Ca and Fe peaks is small for wheat but larger for gardenia. These results imply that indeed the Na content is changing significantly more than that of other elements due to the drought stress experienced by the plants. The relative contents of Na/Fe and Na/Ca are larger and smaller, respectively, in gardenia than in wheat. This behavior indicates different possible mechanisms of stress response in these two different plant species.

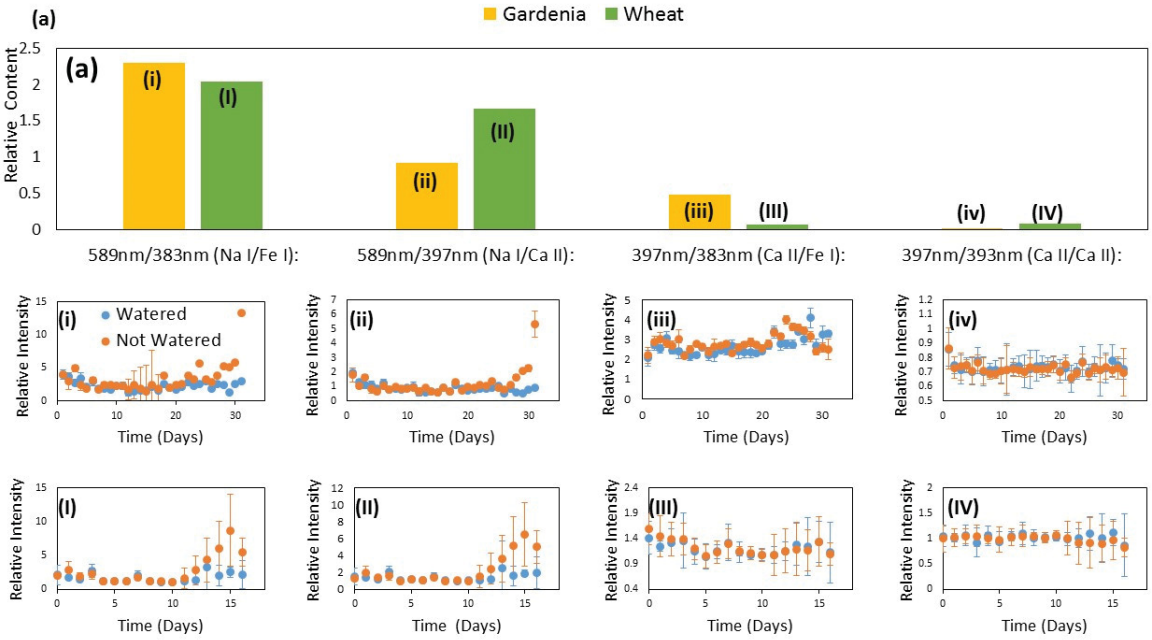

Figure 3.4. Temporal evolution of relative nutrient concentrations. (a) Difference in peak ratios (rms) between watered and non-watered plants for the selected Na, Ca and Fe elements observed in the LIBS spectra of gardenia (yellow bars) and wheat (green bars) plants. Temporal evolution of relative nutrient concentrations of the watered (blue circles) and non-watered (orange circles) gardenia (i) – (iv) and wheat (I) – (IV) plants during the entire treatment periods.

Discussion

Stress within a plant is any unfavorable conditions or substances which negatively affects or inhibits the plant's metabolism and may be short-term or long-term [36]. Plants react differently to stress events depending upon which stress response phase. Certain stress effects can be partially offset for by acclaimation, adaptation and repair mechanisms for minor or accute stress. Chronic or strong stress can cause irreversible damage or may lead to death of the plant [36]. On a small scale, visual inspection of crops may be performed to determine the overall health of field crops. However, for large areas of vegetation, visual inspection is time consuming and sometimes impractical [10,12,37]. The LIBS approach has many advantages for rapid detection of plant stress that allow for this technique to be expanded to the field scale. LIBS can be performed on whole plants without any sample preparation. Additionally, LIBS requires few optical components. Because of these key features, LIBS has the potential to be performed remotely via drone/UAV, allowing for rapid monitoring of vast crop terrain.

Due to the relative simplicity of the method and the ability to monitor elemental contents in plants on the laboratory and field scales, LIBS has the potential to offer insights into the complex mechanisms of plant tolerance and stess response such as the relative K and Na level dynamics, Ca accumulation and transport, and many others. Optimal K^+/Na^+ ratio is crucial for plant metabolism and plays an important role in the osmotic adjustment and stress tolerance under drought and salinity [8,39]. For example, a significant increase of K^+ and Na^+ was reported under drought [39,40,41]. High tolerance to the combined drought and salinity stress was previously related to the lower Na^+/K^+ ratio [42]. Our results indicate an increase in the relative content Na/K ratio in wheat.

Drought and salinity can also affect Ca2+ content [4,41,43]. Further, water deprivation has been shown to damage the mechanism controlling Fe uptake which leads to increased Fe concentraiton in the chloroplasts[44]. LIBS may provide a better understanding of the role of these ions in the stress response. Although the LIBS technique is realtively simple, the interperpation of the data can be complex due to the many factors that effect the sample matrix and plasma conditions. Therefore, the observed LIBS signals are due to the contributions of the changing elemental contents and to the changes in the sample matrix brought about by the induced drought stress. Both factors may be considered as signatures of the drought stress and may be used for the rapid detection of stress in plants.

Our experimental implimentation of LIBS can be further improved by optimizing several parameters such as the lens-to-sample (LTS) distance which plays a minor role for long focal length lenses due to the gradual nature of the focus and increase in the focal volume [13]. Therefore, the LTS can be optimized for stand-off field applications. The detector sensitivity and spectral efficiency are additional control parameters which determine the effectiveness of LIBS in monitoring plant stress. Higher resolution detectors are useful for deconvoluting overlaping atomic species in the LIBS spectra and may provide more precise measurements. Moreover, high resolution detectors allow for monitoring of a larger number of atomic species. LIBS signal strength can be increased using detectors with greater sensitivity and better collection efficiency over large distances or in the presence of background. The benefits of the improved resolution and sensitivity must be balanced with the augmented size and cost of the detector in order to maintain feasability of field applications. Here we used a lightweight inexpensive spectrometer (OceanOptics HR2000) which is suitable for the use on a UAV. For

comparison, we also performed LIBS measurements using a high resolution spectrometer (IsoPlane, Princeton Instruments) and obtained similar results (not shown). In addition to compact spectrometers, compact femtosecond lasers are also available which are suitable for UAV use; however, they are limited in power output. More powerful lasers can be used to increase the signal strength of LIBS or to generate femtosecond plasma filaments which can be used for filament-induced breakdown spectroscopy (FIBS) [45]. FIBS may provide similar information as LIBS with the advantage of longer standoff detection range. Field-scale filament-based environmental analysis was previously performed on a vehicle platform (TERAMOBIL) [46]. It is envisioned that similar technology may be developed for agricultural applications.

In addition to the monitoring of drought stress, the LIBS method can be expanded to include elemental signals of other types of stress and to include other economically meaningful plant species. LIBS may be performed on a large scale in different environments and may be used for comparative field studies between different countries [47]. LIBS may be used to determine spectroscopic signatures of a plethora of stressors for different crops, thereby allowing for greater understanding of the mechanisms of, and improved response to, stress factors found in plant life.

Methods

Sample preparation

Four gardenia plants were purchased from a local nursery and kept indoors at approximately 72^{o} F (day and night) with an irradiance of approximately 9 W m^{-2} from conventional fluorescent tubes. Out of the four gardenia plants, two were randomly

chosen to be stressed (received no water) and the other two not to be stressed (received ~10 ounces of tap water daily). The plant mass was recorded daily using a digital scale (Cen-Tech) as shown in Fig. 1(b). Leaves from the end of the branch were selected to ensure approximately equal maturity and treatment levels. Twenty LIBS spectra were taken on both sides of the central vein in the leaf. Each spectrum was normalized to the LIBS signal at 500 nm for convenience. All twenty spectra were then averaged to obtain a single averaged spectrum for each plant/leaf on each day of the treatment period. Therefore, each individual spectrum shown in Fig. 2 is an average of twenty normalized spectra. Due to uneven distribution of the level of drought stress experienced by each leaf, the spectral intensities showed daily fluctuations. These intensities were determined from the maximum values of the normalized averaged spectra for each observed peak. The sample leaves were separated from the plant stem using scissors and were mounted onto the xyz-translation stage to insure sample flatness and uniformity of LTS distance. No additional sample preparations were made. This methodology may be extended for measuring LIBS spectra of leaves in situ by using an auto-focusing system. Fresh masses of gardenia plants on day 1 were 6595 ± 5 g and 5545 ± 5 g for the watered and non-watered plants, respectively.

The wheat was grown in 0.47 L black plastic pots (Dillen Products, Middlefield, OH). We utilized metro mix 900 for the potting media (Sun Gro Horticulture Canada Ltd, Vancouver, BC), starting on 13 Nov 2014, and fertilizing weekly with approximately 450 ppm nitrogen (Peters Professional 20N-8.74P-16.6K, Scotts Co., Marysville, Ohio). Plants were grown in a plastic greenhouse without light exclusion, with temperature set points of 85^{o} F day and 75^{o} F night. Ten wheat pots (with ~10 plants per

pot) were randomly selected to receive water and the other 10 pots were selected not to receive water. Every pot containing wheat plants in the watered (mild stress) group received water daily to keep the soil moisture level constant. There was a mild lighting stress in the watered wheat group. Plants from the non-watered (severe drought stress) group received no water. Their masses were recorded daily using the same digital scale for all pots containing wheat plants separately and were then averaged for the group [Fig. 1(d)]. One sample leaf was selected from each pot (middle leaf of an individual wheat sprout) that represented the state of the whole pot and then all spectra from the 10 representative wheat leaves were averaged and plotted as a single averaged spectrum. Average wheat masses on day 1 were 296 ± 26 g and 274 ± 29 g for the watered and non-watered treatment groups, respectively.

Laser-induced breakdown spectroscopy (LIBS)

LIBS experiments were performed using a femtosecond laser system consisting of a mode-locked Ti:Sapphire laser oscillator (Tsunami, Spectra Physics) operating at ~ 800 nm center wavelength, with a pulse duration of ~ 35 fs FWHM and an amplifier (TSA, Spectra Physics) operating at a repetition rate of 1 kHz. The samples were placed on a xyz-translation stage to ensure that a fresh surface was ablated. Translation of the sample in the beam path took place at a rate of approximately 1 cm/s. The incident beam was attenuated to 300 mW (0.3 mJ pulse energy) by a neutral density filter and was then focused onto the sample surface by a 50 mm focal length lens. A color glass filter was used to suppress the pump beam reflection. The LIBS spectra were collected at a 45º angle and measured using an Ocean Optics HR2000 spectrometer as shown in Fig. 5. No time delay between excitation and spectral measurements was employed. All LIBS

measurements were performed at ambient conditions. LTS distance was optimized daily utilizing a reference sample to insure system stability.

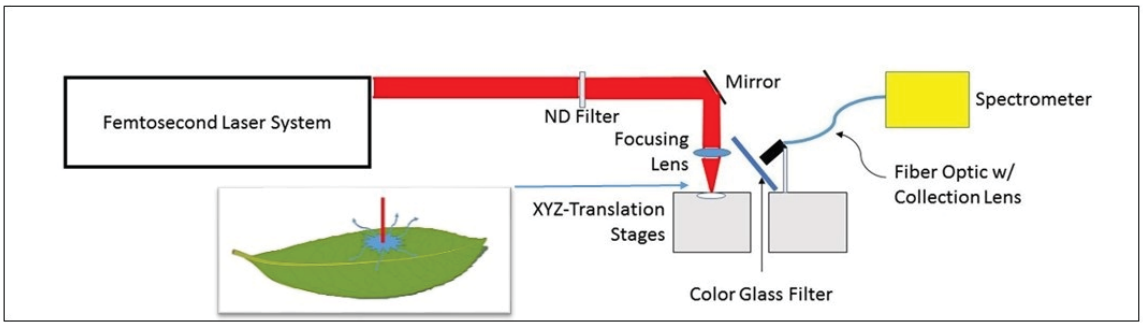

Figure 3.5. Schematic of the laser-induced breakdown spectroscopy (LIBS) performed on a leaf sample (inset).

Plasma temperature measurement

Assuming that the plasma is in local thermal equilibrium (LTE) and optically thin [13,48], the Boltzmann distribution method was used to determine the plasma temperature. The intensity of a given LIBS spectral line is:

$$I = \frac{h\upsilon AN}{4\pi} = \left(\frac{hcN_0gA}{4\pi\lambda Z}\right) e^{-\left(\frac{E}{k_bT}\right)}, \quad (1)$$

where h is Planck's constant, υ is the frequency of the emitted radiation, A is the transition probability, N is the number of particles involved in the transition, c is the speed of light in vacuum, N_0 is the total population of the species, λ is the wavelength of the emitted radiation, g is the statistical weight, Z is the partition function, E is the transition energy, k_b is Boltzmann's constant, and T is the temperature [13]. Equation (1) can be rearranged as:

$$\ln\left(\frac{I\lambda}{gA}\right) = -\frac{E}{k_bT} - \ln\left(\frac{4\pi Z}{hcN_0}\right), \quad (2)$$

from which the plasma temperature was obtained from the inverse of the slope of the best-fit-line of $\ln(I\lambda/gA)$ vs. E. The transition energies E and intensities I were determined from the LIBS spectra utilizing the Ca I spectral lines. The g and A values were taken from the NIST database [34]. The uncertainty of the plasma temperature measurements is mainly determined by the uncertainties of the relative line intensity (I) and the transition probability (A) measurements [49]. The latter is often neglected (see for example p. 130 in ref. [50]) and was assumed negligible in our analysis. The uncertainties in Ca I transition probabilities in our detectable range may vary between 2% and 50% depending on the selected transitions, and adding more data points to the Boltzmann plot reduces the corresponding uncertainty.

Funding

National Science Foundation (NSF) (PHY-1307153); the Office of Naval Research (ONR) (N00014-16-1-3054, N00014-16-1-2578); the Robert A. Welch Foundation (A-1261, A-1547).

Acknowledgments

Wheat plants were provided by Sean Carver of Texas A&M University.

1. V. Vassileva, D. Demirevska, L. Simova-Stoilova, T. Petrova, N. Tsenov, and U. Feller, "Long-Term Field Drought Affects Leaf Protein Pattern and Chloroplast Ultrastructure of Winter Wheat in a Cultivar-Specific Manner," J. Agronomy & Crop Science **198**, 104-117 (2012).
2. H. W. Koyro, P. Ahmad, and N. Geissler, "Abiotic stress responses in plants: an overview," *in Environmental Adaptations and Stress Tolerance of Plants in the Era of Climate Change*, Eds.: P. Ahmad and M. N.V. Prasad. (2012).
3. M. Farooq, M. Hussain, A. Wahid, and K. H. M. Siddique, "Drought stress in plants: an overview," *in Plant Responses to Drought Stress*, Ed.: R. Aroca. (2012).
4. S. S. Gill, N. A. Anjum, R. Gill, and N. Tuteja, "Abiotic stress signaling in plants – an overview," in *Abiotic Stress Response in Plants,* Eds.; N. Tuteja and S. S. Gill. (2016).
5. L. Chaerle, W. Van Caeneghem, E. Messens, H. Lambers, M. Van Montagu, and D. Van Der Straeten, "Presymptomatic visualization of plant–virus interactions by thermography," Nature Biotechnology **17**, 813-816 (1999).
6. H. G. Jones, "Use of thermography for quantitative studies of spatial and temporal variation of stomatal conductance over leaf surfaces," Plant, Cell and Environment **22**, 1043-1055 (1999).
7. J. Peñuelas, and I. Filella, "Visible and nearinfrared reflectance techniques for diagnosing plant physiological status," Trends Plant Sci. **3**, 151-156 (1998).
8. J. J. Casanova, S. A. O'Shaughnessy, S. R. Evett, and C. M. Rush, "Development of a wireless computer vision instrument to detect biotic stress in wheat," Sensors **14**, 11153 (2014).
9. K. Hancke, B. K. Sorell, L. C. Lund-Hansen, M. Larsen, T. Hancke, and R. N. Glud, "Effects of temperature and irradiance on a benthic microalgal community: A combined two-dimensional oxygen and fluorescence imaging approach," Limnol. Oceanogr **5**, 1599-1611 (2014).
10. H. K. Lichtenthaler, and F. Babani, "Detection of photosynthetic activity and water stress by imaging the red chlorophyll fluorescence," Plant Physiol. Biochem. **38**, 889-895 (2000).
11. R. B. Peterson, and D. E. Aylor, "Chlorophyll Fluorescence lnduction in Leaves of Phaseolus vulgaris Infected with Bean Rust (Uromycesappendiculatus)," Plant Physiol. **108**, 163-171 (1995).
12. A. Porcar-Castell, E. Tyystjarvi, J. Atherton, C. van der Tol, J. Flexas, E. E. Pfundel, J. Moreno, C. Frankenberg, and J. A. Berry, "Linking chlorophyll a fluorescence to photosynthesis for remote sensing applications: mechanisms and challenges," Journal of Experimental Botany **65**, 4065-4095 (2014).

13. D. A. Cremers, and L. J. Radziemski, *Handbook of Laser-Induced Breakdown Spectroscopy* (John Wiley & Sons Ltd., West Sussex, UK, 2006).

14. R. Kanawade, F. Mahari, C. Klampfl, M. Rhode, C. Knipfer, K. Tangermann-Gerk, W. Adler, M. Schmidt, and F. Stelzle, "Qualitative tissue differentiation by analysing the intensity ratios of atomic emission lines using laser induced breakdown spectroscopy (LIBS): prospects for a feedback mechanism for surgical laser systems," J. Biophotonics **8**, 153-161 (2015).

15. D. Marcos-Martinez, J. A. Ayala, R. C. Izquierdo-Hornillos, F. J. Manuel de Villena, and J. O. Caceres, "Identification and discrimination of bacterial strains by laser induced breakdown spectroscopy and neural networks," Talanta **84**, 730-737 (2011).

16. A. C. Samuels, F. C. DeLucia Jr., K. L. McNesby, and A. W. Miziolek, "Laser-induced breakdown spectroscopy of bacterial spores, molds, pollens, and protein: initial studies of discrimination potential," Applied Optics **42**, 6205-6209 (2003).

17. B. Bousquet, G. Travalle, A. Ismael, L. Canioni, K. Michel-Le Pierres, E. Brasseur, S. Roy, I. Le Hecho, M. Larregieu, S. Tellier, M. Potin-Gautier, T. Boriachon, P. Wazen, A. Diard, and S. Belbeze, "Development of a mobile system based on laser-induced breakdown spectroscopy and dedicated to in situ analysis of polluted soils," Spectrochimica Acta Part B **63**, 1085-1090 (2008).

18. D. Diaz, D. W. Hahn, and A. Molina, "Evaluation of Laser-Induced Breakdown Spectroscopy (LIBS) as a Measurement Technique for Evaluation of Total Elemental Concentration in Soils," Applied Spectroscopy **66**, 99-106 (2012).

19. O. Samek, J. Lambert, R. Hergenroder, M. Liska, J. Kaiser, K. Novotny, and S. Kukhlecsky, "Femtosecond laser spectrochemical analysis of plant samples," Laser Phys. Lett. **3**, 21-25 (2006).

20. D. Sun, S. Maugen, C. Dong, and X. Ma, "A semi-quantitative analysis of essential micronutrient in folium lycii using laser-induced breakdown spectroscopy technique," Plasma Science and Technology **12**, 478 (2010).

21. D. Santos Jr., L. C. Nunes, G. G. A. Carvalho, and F. J. Krug, "Laser-induced breakdown spectroscopy for analysis of plant materials: a review," Spectrochimica Acta B **71**, 3 (2012).

22. J. Kaiser, K. Novotny, M. Z. Martin, A. Hrdlicka, R. Malina, M. Hartl, V. Adam, and R. Kizek, "Trace elemental analysis by laser-induced breakdown spectroscopy – biological applications," Surface Science Reports **67**, 233 (2012).

23. K. Devey, M. Mucalo, G. Rajendram, and J. Lane, "Pasture vegetation elemental analysis by laser-induced breakdown spectroscopy," Communications in Soil Science and Plant Analysis **46**, 72 (2015).

24. G. G. A. Carvalho, J. Moros, D. Santos Jr., F. J. Krug, and J. J. Laserna, "Direct determination of the nutrient profile in plant material by femtosecond laser-induced breakdown spectroscopy," Analytica Chimica Acta **876**, 26-38 (2015).

25. H. Chen, H. Li, Y. C. Sun, Y. Wang, and P. J. Lu, "Femtosecond laser for cavity preparation in enamel and dentin: ablation efficiency related factors," Scientific Reports **6**, 1-8 (2016).

26. Z. Dong, X. Zhou, J. Wu, Z. Zhang, T. Li, Z. Zhou, S. Zhang, and G. Li, "Small incision lenticule extraction (SMILE) and femtosecond laser LASIK: comparison of corneal would healing and inflammation," Br J Opthalmol **0**, 1-7 (2013).

27. A. A. Farjo, A. Sugar, S. C. Schalhorn, P. A. Majmudar, D. J. Tanzer, W. B. Trattler, J. B. Carson, K. E. Donaldson, and G. D. Kymionis, "Femtosecond laser LASIK flap creation: a report by the American academy of ophthalmology," Ophthalmology **120**, e5-e20 (2013).

28. F. Chen, and J. R. Vazquez de Aldana, "Optical waveguides in crystalline dielectric materials produced by femtosecond-laser micromachining," Laser Photonics Rev. **8**, 251-275 (2014).

29. G. Vocke, United States Department of Agriculture Economic Research Service, http://www.ers.usda.gov/topics/crops/wheat.aspx (2016).

30. A. Assion, M. Wollenhaupt, L. Haag, F. Mayorov, C. Sharpe-Tudoran, M. Winter, U. Kutschera, and T. Baumert, "Femtosecond laser-induced-breakdown spectrometry for Ca2+ analysis of biological samples with high spatial resolution," Appl. Phys. B **77**, 391 (2003).

31. M. Bossu, H. Zuo-Qiang, M. Baudelet, Y. Jin, Z. Zhe, and Z. Jie, "Femtosecond Laser-Induced Breakdown Spectroscopy for Detection of Trace Elements in Sophora Leaves," Chin. Phys. Lett. **24**, 3466 (2007).

32. G. G. A; Carvalho, D. Santos Jr., L. C. Nunes, M. Silva Gomes, F. Oliveira Leme, and F. J. Krug, "Effects of laser focusing and fluence on the analysis of pellets of plant materials by laser-induced breakdown spectroscopy," Spectrochimica Acta Part B **74-75**, 162-168 (2012).

33. M. Galiova, J. Kaiser, K. Novotny, O. Samek, L. Raele, R. Malina, K. Palenikova, M. Liska, V. Cudek, V. Kanicky, V. Otruba, A. Poma, and A. Tucci, "Utilization of laser-induced breakdown spectroscopy for investigation of metal accumulation in vegetal tissue," Spectrochimica Acta Part B **62**, 1597 (2007).

34. A. Kramida, Y. Ralchenko, J. Reader, and NIST ASD Team, NIST Atomic Spectra Database (ver. 5.2), http://physics.nist.gov/asd (2016).

35. E. Epstein in *Plant Biochemistry* (Eds Bonner, J. & Varner, J. E.) 438 (Academic, London, 1965).

36. H. K. Lichtenthaler, "Vegetation stress: an introduction to the stress concept in plants," J. Plant Physiol **148**, 4-14 (1995).

37. L. J. Wiles, H. J. Gold, and G. G. Wilkerson, "Modeling the uncertainty of weed density estimates to improve post-emergence herbicide control decisions," Weed Research **33**, 241-252 (1993).

38. T. J. Flowers, and A. R. Yeo, "Ion relations in plants under drought and salinity," Aust. J. Plant Physiol. **13**, 75 (1986).

39. I. Slama, T. Ghnaya, A. Savoure, and C. Abdelly, "Combined effects of long-term salinity and soil drying on growth water relations, nutrient status and proline accumulation," C R Biol. **331**, 442 (2008).

40. J. P. Martinez, J. F. Ledent, M. Bajji, J. M. Kinet, and S. Lutts, "Effect of water stress on growth, Na+ and K+ accumulation and water use efficiency," Plant Growth Regulation **41**, 63 (2003).

41. J. M. Pardo, and F. J. Quintero, "Plants and sodium ions: keeping company with the enemy," Genome Biology **3**, 1017 (2002).

42. I. M. Ahmed, F. Cao, M. Zhang, X. Chen, G. Zhang, and F. Wu, "Difference in yield and physiological features in response to drought and salinity," PLOS One **8**, e77869 (2013).

43. H. Knight, A. Trewavas, and M. R. Knight, "Calcium signalling in Arabidopsis thaliana responding to drought and salinity," Plant J. **12**, 1067 (1997).

44. A. H. Price, and G. A. F. Hendry, "Iron-catalysed oxygen radical formation and its possible contribution to drought damage in nine native grasses and three cereals," Plant, Cell and Environment **14**, 477-484 (1991).

45. J. P. Singh, and S. N. Thakur, *Laser-Induced Breakdown Spectroscopy* (Elsevier, Amsterdam, Netherlands, 2007).

46. G. Mejean, J. Kasparian, J. Yu, S. Frey, E. Salmon, and J. P. Wolf, "Remote detection and identification of biological aerosols using a femtosecond terawatt lidar system," Appl. Phys. B **78**, 535-537 (2004).

47. L. Eleuch, A. Jilal, S. Grando, S. Ceccarelli, M. Schmising, H. Tsujimoto, A. Hajer, A. Daaloul, and M. Baum, "Genetic diversity and association analysis for salinity tolerance," J. Integ. Plant Biol. **50**, 1004 (2008).

48. W. Lei, V. Motto-Ros, M. Boueri, Q. Ma, D. Zhang, L. Zheng, H. Zeng, and J. Yu, "Time-resolved characterization of laser-induced plasma from fresh potato," Spectrochimica Acta Part B **64**, 891-898 (2009).

49. S. Zhang, X. Wang, M. He, Y. Jiang, B. Zhang, W. Hang, and B. Huang, "Laser-induced plasma temperature," Spectrochimica Acta Part B **97**, 13-33 (2014).

50. A. W. Miziolek, V. Palleschi, and I. Schechter, *Laser-Induced Breakdown Spectroscopy (LIBS): Fundamentals and Applications* (Cambridge University, Cambridge, UK, 2006).

CHAPTER FOUR

Interaction of Femtosecond Laser Pulses with Plants: Towards Distinguishing Weeds and Crops using Plasma Temperature

This chapter published as: J.N. Kunz, D.V. Voronine, B.A. Ko, H.W. Lee, A. Rana, M.V. Bagavathiannan, A.V. Sokolov and M.O. Scully, "Interaction of femtosecond laser pulses with plants: towards distinguishing weeds and crops using plasma temperature," *Journal of Modern Optics*, vol. 64, pp. 942-947, 2017.

Abstract

The ability to distinguish between crops and weeds using sensors from a distance will greatly benefit the farming community through improved and efficient scouting for weeds, reduced herbicide input costs and improved profitability. In the present study, we examined the utility of femtosecond laser-induced breakdown spectroscopy (LIBS) for plant species differentiation. Greenhouse-grown plants of dallisgrass, wheat, soybean and bell pepper were evaluated using LIBS under an ambient environment. LIBS experiments were performed on the leaf samples of different plant species using a femtosecond laser system with an inexpensive lightweight detector. Temperatures of laser-induced plasmas in plants depend on many parameters and were determined for each of the study species by the constituent elements interacting with femtosecond laser pulses. Using elemental calcium transitions in plant tissue samples to measure plasma temperatures, we report consistent differences among the four study species, with average values ranging from 5,090 ± 168 K (soybean) to 5,647 ± 223 K (dallisgrass).

Introduction

In agriculture, the ability to distinguish between crops and weed species from a distance using sensors has enormous practical applications. Growers and crop consultants typically spend numerous hours each growing season scouting for the presence of weeds in production fields because effective weed management and crop yield protection relies on timely identification of weed issues and taking appropriate management decisions based on weed assessments [1]. Routine scouting for weeds serves as an important component of herbicide-resistance best management practices [2]. According to a recent report produced by the United States Department of Agriculture, scouting for weeds was the most widely practiced crop monitoring service in several crops [3]. Manual field scouting is not only an expensive and time-consuming process, but is inaccurate and often hampered by adverse weather conditions. Given the recent technological advancements in the arena of unmanned ground vehicles (UGVs) and unmanned aerial vehicles (UAVs), there is a possibility for carrying a suit of sensors and scout for weeds from above crop canopies at much higher precision and efficiency. While integration of various sensors with UGV/UAV platforms is continuing to evolve and payload limitations are being overcome, it is critical that targeted experiments are conducted under controlled environments to fully understand the capabilities and limitations of a diverse set of sensor tools for use in specific applications. For weed scouting applications, researchers have traditionally investigated tools such as GreenSeekers [4,5], LIDAR [6,7], Ultrasonic sensors [8,9], DSLR cameras [10], multispectral cameras [11,12] and, in some cases, hyperspectral sensors [13,14].

The LIBS technology, widely employed in many industries for real-time monitoring of elemental and chemical composition [15,16,17], may have a great potential for use in plant species differentiation. Because LIBS is a simple but versatile modality, it has been applied in a host of analytical pursuits ranging from distinguishing between bacterial strains [18], analysis of meteorites and the Martian surface [19], and the dating of archeological findings [19] to the classification of Chinese tea leaves [20], soil analysis [19,21], and food science applications [22,23,24]. In particular, LIBS performs well in detecting minerals and metals, and is therefore an attractive technology for food process monitoring including: examining Ca in poultry processing [22], Pb and Si in wheat seedlings [23], and Na in baked goods [24]. LIBS has also been used in more fundamental capacities of food science in which nutrients and pesticides of raw agricultural products are analysed [25]. During LIBS, the focused femtosecond laser pulses interact with the sample, vaporizing a small volume, and forming a plasma plume. The hot plasma breaks down the vaporized material into atomic components and excites electrons into higher energy states. As the plasma cools and expands, the electrons return to the ground state and emit photons at unique atomic frequencies [15].

Within the broad applications of LIBS, there is much flexibility in the performance of the technique. Pulses used for ablation of small amounts of sample surface can be obtained from nano-, pico-, and femtosecond lasers. Femtosecond pulses are of particular interest because high powers can be obtained with smaller energies; therefore, resulting in less damage to the sample [15]. Additionally, shorter pulse lengths allow for less interaction of the pulse with the formed plasma, causing a reduction in broad continuum background noise [15]. Femtosecond laser pulses have been used in

plant science applications [26,27,28], medical purposes, such as in dentistry cavity preparation [29] and LASIK surgery [30,31], and micromachining [32]. In particular, femtosecond laser pulses were found to yield more accurate results for applications where plant samples were employed due to the lower continuum background [26].

While there have been many studies using LIBS as a detection tool, an underutilized property of the technique is the use of the plasma temperature during ablation. The temperature of the plasma produced during LIBS depends on a number of factors, from pulse length and wavelength of the excitation laser to the angle of incidence and the composition of the sample [16]. During LIBS, a portion of the laser pulse energy is used to vaporize and ionize the sample. This required fraction depends on the molecular composition of the sample. After vaporization and ionization, the remaining portion of the laser pulse heats the plasma [17].

In the LIBS of plant matter, such as leaves, the plasma temperature will strongly depend on the molecular chemical composition. As most plants share common compounds; such as lignin [33] and cellulose [34], their different relative concentrations will result in a difference in the required energy to ionize the sample. Thus, the remaining pulse energy that heats the resultant plasma and excites the atomic and ionic transitions varies, and the measured peak ratios in the LIBS spectra characteristic of the plant species. The plasma temperature also depends on water concentration, as vacuole size affects the proportions of these compounds. Therefore, dried samples are preferred when measuring plasma temperature of different species in order to reduce the effects of water concentrations.

Several methods exist for the determination of the laser-induced plasma (LIP) temperature. Among the most common are the Boltzmann method, the Saha-Boltzmann method, the line-to-continuum method, and the synthetic spectra method [35]. The first two methods are quantum mechanical in nature and utilize the LIBS spectral line intensities in determining the LIP temperature; whereas, the line-to-continuum method is semi-classical and exploits the continuum background in addition to the spectral line intensity [35]. The synthetic spectra method is mainly used to find the molecular temperature which is related to the heavy particle gas temperature [35]. Here we performed femtosecond LIBS measurements which allowed for distinguishing between four plant species based on the laser-induced plasma temperature determined using the Boltzmann method. Our results may be extended to field-scale standoff LIBS.

Materials and Methods

LIBS experiments were performed on two monocot (dallisgrass, *Paspalum dilatatum*; wheat, *Triticum aestivum*) and two dicot species (soybean, *Glycine max*; bell pepper, *Capsicum annuum*). Among these, dallisgrass is a troublesome in lawns and home gardens weed, whereas the other three are crop species. The crop and weed species were established under greenhouse conditions in pots (15 cm dia x 10 cm deep) filled with potting soil mix (LC1, SunGro Horticulture, Canada). The greenhouse was maintained at day/night temperature cycles of 30/25 C and 16 hr photoperiod. Plants were irrigated and fertilized (Miracle-Gro®, Scotts Company) as required. A total of two plants were established for each study species and were maintained in the greenhouse until they reached about 10-15 cm tall growth stage, prior to conducting LIBS evaluations.

LIBS experiments were performed using a femtosecond laser system consisting of a mode-locked Ti:Sapphire laser oscillator (Tsunami, Spectra Physics) operating at ~ 800 nm center wavelength, with a pulse duration of ~ 35 fs FWHM and a 1 kHz repetition rate amplifier (TSA, Spectra Physics). One dry plant leaf sample was placed on a xyz-translation stage to ensure that a different surface was ablated with each spectrum recorded. The incident beam was attenuated to 300 mW (0.3 mJ per pulse) by a neutral density filter and was then focused onto the sample surface by a 50 mm focal length lens. The laser spot size on the sample surface was ~ 100 μm. The corresponding irradiance (fluence) was ~ 3.8 kW/cm^2 (3.8 J/cm^2 per pulse). A color glass filter was used to suppress the pump beam reflection. The collecting optics for the LIBS spectral measurements consisted of an uncoated plano-concave lens placed at ~ 5 cm distance from the sample surface at a 45º angle with respect to the incident laser beam and an Ocean Optics HR2000 spectrometer with a 600 groves/mm grating (Ocean Optics HC-1) and 2048 element CCD array with ~ 1 nm spectral resolution in the 200 nm to 800 nm wavelength range without any time delay [Figure 4.1]. All LIBS measurements were performed in an ambient environment. All leaf samples were removed from plants using a pair of shears, dried for ~24 hours, and then mounted onto the xyz-translation stage with no additional sample preparation. Ten LIBS spectra were recorded and averaged from a single leaf from each of the two replicates of each studied species using 500 laser pulses per spectrum with 0.5 s integration time. The number of sampling points of the leaf surface is estimated to be ~ 100 based on the ratio of the ~ 10 mm length of the continuously scanned area of the leaf between the center stem and the outer edge of the

leaf to the size of the laser spot. Intensities for the relevant calcium peaks were recorded and used to determine the plasma temperatures for the four different study species.

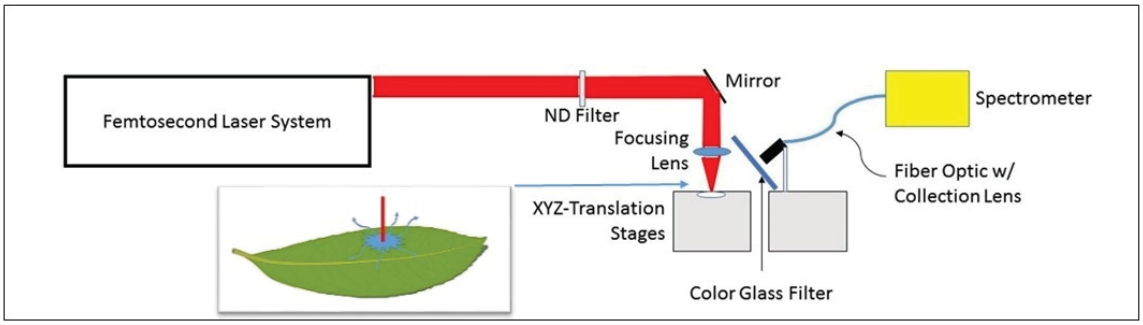

Figure 4.1. Schematic of the laser-induced breakdown spectroscopy (LIBS) performed on a leaf sample (inset).

Results

Typical LIBS spectra for each of the four plant varieties are shown in Figure 4.2, where each spectrum was normalized and offset for convenience. In each spectra, Na, Ca, and Fe were observed and corresponding peaks were identified. Additionally, the three Ca I peaks used for plasma temperature calculations are highlighted for all four plant species. Ca was selected for the determination of the plasma temperature because several strong Ca transitions were observed in the LIBS spectra of all the four investigated plant species providing enough data points for the Boltzmann plots.

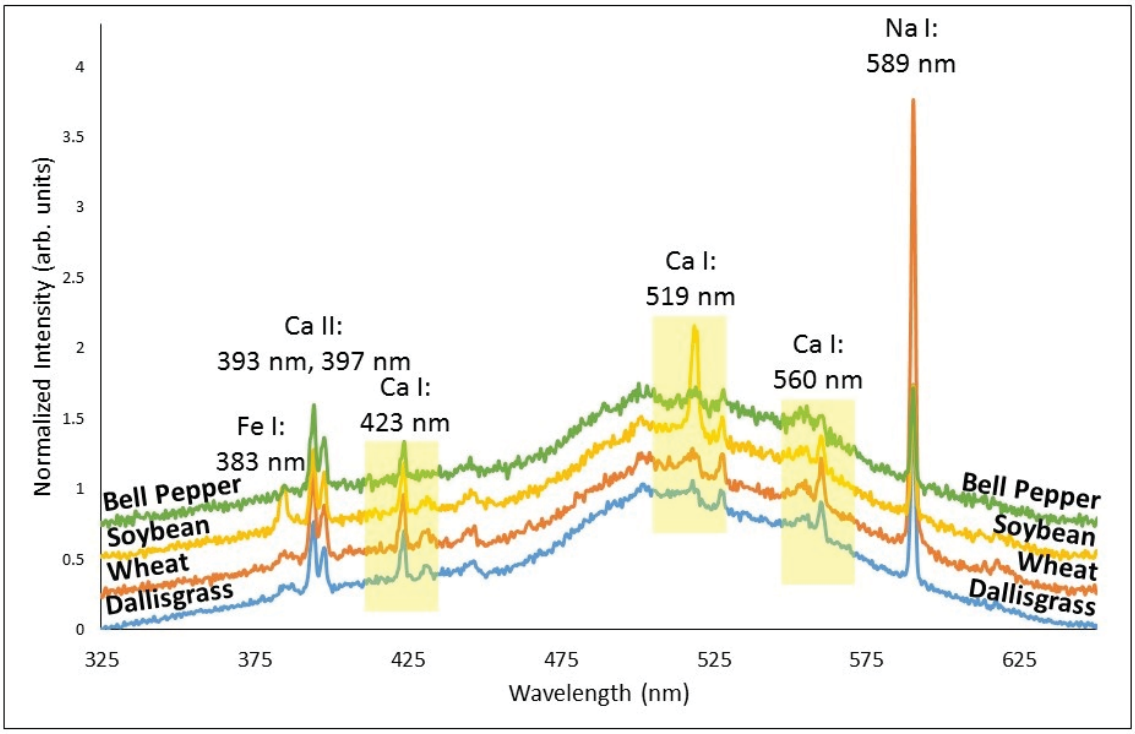

Figure 4.2. LIBS spectra of the four plant species: three crops (bell pepper, soybean and wheat) and a weed (dallisgrass). The major peaks are labeled by the corresponding element and emission wavelength. Three calcium peaks used for calculation of the plasma temperature are highlighted. The spectra are normalized to the 500 nm signal and vertically shifted for convenience.

Assuming optically thin plasma at local thermal equilibrium (LTE), the Boltzmann distribution method was used to determine the plasma temperature [15]. The intensity of a given spectral line in the LIBS spectra is

$$I = \frac{\mathrm{h}\upsilon \mathrm{AN}}{4\pi} = \left(\frac{\mathrm{hc}N_0 \mathrm{gA}}{4\pi\lambda \mathrm{Z}}\right) e^{-\left(\frac{E}{k_b T}\right)}, \quad (1)$$

where I is the maximum intensity of the LIBS signal of a selected transition, h is Planck's constant, υ is the frequency of the emitted radiation, A is the transition probability, N is the number of particles involved in the transition, c is the speed of light in vacuum, N_0 is the total population of the atomic species, λ is the wavelength of the emitted radiation, g is the statistical weight, Z is the partition function, E is the energy of the upper state for

the radiant transition, k_b is Boltzmann's constant, and T is the plasma temperature [15]. Rearranging Eq. 1 in the form

$$\ln\left(\frac{I\lambda}{gA}\right) = -\frac{E}{k_b T} - \ln\left(\frac{4\pi Z}{hcN_0}\right) \quad (2)$$

we determined the plasma temperature from the inverse of the slope of the best-fit-line (Figure 4.3).

Figure 4.3 shows the Boltzmann plots of the average LIBS peak intensities of Ca I transitions and best-fit-lines used to calculate the plasma temperatures for each of the leaf samples and the corresponding photographs of the leaves. The numerical values of the parameter used for these plots are given in Table 4.1 and were obtained from the NIST database for atomic spectra [36] and from the LIBS measurements. The data fit quality limited by the number of available data points (only three peaks observed for Ca I in the LIBS spectra in Figure 4.2), spectral resolution of the detector (higher resolution helps deconvoluting overlap contributions of other species), broad background and LIBS fluctuations. The uncertainty of the plasma temperature measurements is mainly determined by the uncertainties of the relative line intensity (I) and the transition probability (A) measurements [35]. The latter is often neglected (see for example p. 130 in ref. [17]) and was assumed negligible in our analysis. The uncertainties in Ca I transition probabilities in our detectable range may vary between 2% and 50% depending on the selected transitions, and adding more data points to the Boltzmann plot reduces the corresponding uncertainty. R^2 values are 0.7, 0.7, 0.6, and 0.7 for dallisgrass, wheat, soybean, and bell pepper leaves, respectively. The fit quality may be improved by optimizing the detection and background subtraction techniques. This may improve the precision of determining the plasma temperature. However, our method yields semi-

quantitative results which allow for distinguishing crops and weeds under identical conditions using relatively inexpensive and simple equipment which may have advantages in field applications.

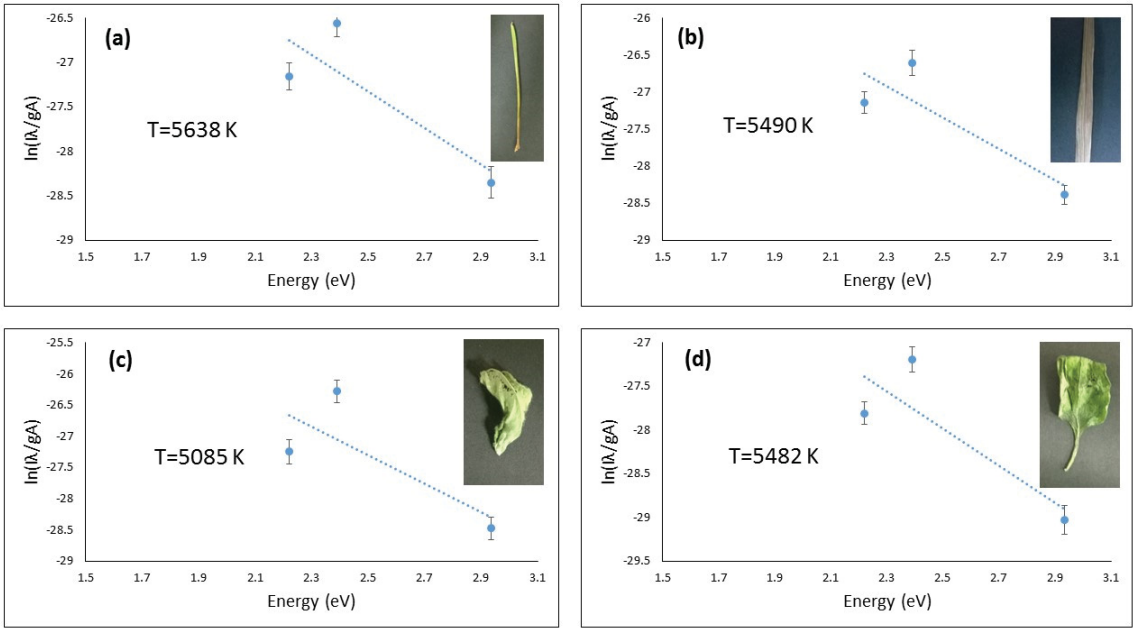

Figure 4.3 Representative Boltzmann plots for Ca I emission lines from the dallisgrass (a), wheat (b), soybean (c), and bell pepper (d) sample leaves. Average plasma temperatures and leaf photographs are shown in the inset.

Figure 4.4 shows the average plasma temperatures from the ten spectra obtained for each of the four plant species. Though typical LIBS measurements of plant materials are performed on homogenious pelletized samples, we carried out measurements on whole leaves for the future extension to field applications. The contribution of sample inhomogeneity to the uncertainty of measurements is included in the error bars in Fig. 4 by averaging the ten spectra measured across the leaf surface. While there is some overlap within the uncertainty limits, the average plasma temperatures are distinct.

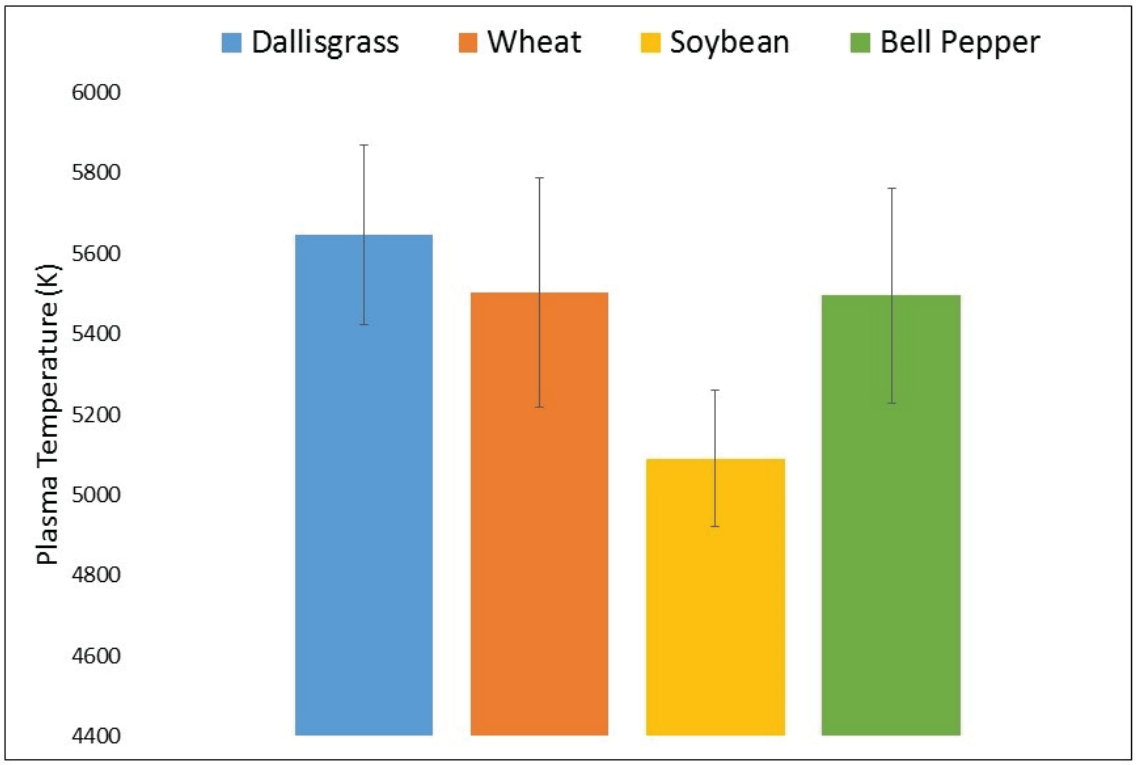

Figure 4.4 Plasma temperatures plotted for each plant.

Discussion

LIBS is a functional technique with many advantages, especially for remote field observations. Here we present a simple method that can distinguish between various plant species, with practical applications for identifying and differentiating crops and weed species. Because most plants share several common elements and compounds, the peaks that appear in the typical LIBS spectra are very similar [see Figure 4.2]. Several modifications can be made to enhance sensitivity and improve the detection limits. One such improvement is that of a higher resolution detector. An addition, using a detector with an extended spectral range would allow for the possibility of collecting and observing other Ca I lines providing more data points for the Boltzmann plots and therefore increasing precision in plasma temperature calculations [35]. Though these

advantages are compelling, one must weigh these benefits against the increased cost and decreased mobility that accompany enhanced detectors. Along with the increased spectral region of the detector, a notch filter in place of the color glass filter in order to suppress the back-scattered laser radiation would provide an extra improvement in resolution and sensitivity and would allow for detecting additional elements in a broader spectral range.

Table 4.1 Spectroscopic data for calcium emission lines used to calculate plasma temperatures obtained from NIST.gov atomic spectral database [22].

Peak Wavelength (nm)	Atomic Species (Listed Transition Wavelength in nm)	E (eV)	gA (s-1)
423	Ca I (422.874)	2.934542	6.54 x 108
519	Ca I (518.542)	2.390426	2.0 x 108
560	Ca I (559.849)	2.21938	3.4 x 108

Further improvements could be achieved by varying the temporal width of the laser pulses. Most LIBS approaches used ns laser pulses for the analysis of plant materials. For example, using the ns LIBS could reduce the cost of the laser system and achieve pulses with energies on the order of a few hundred mJ which may generate hotter plasma with more detectable elements in the plant material. This would require using detectors with a time delay to suppress the continuum background which was shown to be lower for fs LIBS [26]. Another advantage of fs LIBS is the higher spatial resolution due to the shorter interaction time, lower laser fluence, reduced plasma temperature and the corresponding decrease of the ablation volume [27,37]. Also both ns and fs LIBS can be used for short-range (up to ~ 100 m) stand-off detection using telescopes [38]. However, fs laser pulses may be used for the generation of laser filaments which are advantageous for long-range (> 100 m) stand-off filament-induced laser breakdown spectroscopy [39].

Additional modifications could be made to use longer delay times between the formation of plasma and LIBS measurements. The plasma temperature at zero delay time may reach high values up to tens of thousands degrees and decrease at longer times. For simplicity we used the zero delay. Our results may be further improved by adding a longer delay time [35].

With the ability to distinguish between plants that look similar, and especially from a distance, growers and crop consultants can effectively scout for the presence of weeds in large production areas within a short time and apply herbicides to specific areas where required, allowing for a reduction in herbicide use and associated environmental impacts and improved profitability.

References

1. Wiles, L.J.; Wilkerson, J.J.; Gold, H.J. Crop Prot. 1992, 11, 547-554.

2. Norsworthy, J.K.; Ward, S.M.; Shaw, D.R.; Llewellyn, R.S.; Nichols, R.L.; Webster, T.M.; Bradley, K.W.; Frisvold, G.; Powles, S.B.; Burgos, N.R.; Witt, W.W.; Barrett, M. *Weed Science.* **2012**, *Special Issue,* 31-62.

3. NASS Agricultural Chemical Use Program 2014. National Agricultural Statistical Service of the United Nations. http://www.nass.usda.gov/Surveys/Guide_to_NASS_Surveys/Chemical_Use/ (accessed April 25, 2016).

4. Walsh, O.S.; Klatt, A.R.; Solie, J.B.; Godsey, C.B. *Precision Agric.* **2013**, *14,* 343-356.

5. Martin, D.E.; Lopez, J.D. Jr.; Lan, Y. *Int J Agric & Biol Eng.* **2012**, *5,* 43-47.

6. Lehoczky, E.; Tamas, J.; Riczu, P.; Herdon, M. Weed mapping based on integrated remote sensing method. *Proceedings in World Conference on Computers in Agriculture and Natural Resources,* University of Costa Rica, San Jose Costa Rica, July 27-30, 2014.

7. Weiss, U.; Biber, P.; Laible, S.; Bohlmann, K.; Zell, A. Plant species classification using a 3d lidar sensor and machine learning. *Proceedings in Machine Learning and Applications (ICMLA), 2010 Ninth International Conference,* Washington D.C., December 12-14, 2010.

8. Andujar, D.; Weis, M.; Gerhards, R. *Sensors.* **2012**, *12,* 17343-17357.

9. Zaman, Q.U.; Esau, T.J.; Schumann, A.W.; Percival, D.C.; Chang, Y.K.; Read, S.M.; Farooque, A.A. *Computers and Electronics in Agriculture.* **2011**, *76,* 175-182.

10. Nijland, W.; de Jong, R.; de Jong, S.M.; Wulder, M.A.; Bater, C.W.; Coops, N.C. *Agricultural and Forest Meteorology.* **2014**, *184,* 98-106.

11. Gerhards, R.; Christensen, S. *Weed Research.* **2003**, *43,* 385-392.

12. Lamb, D.W.; Weedon, M.M.; Rew, L.J. *Weed Research.* **1999**, *39,* 481-492.

13. Hestir, E.L.; Khanna, S.; Andrew, M.E.; Santos, M.J.; Viers, J.H.; Greenberg, J.A.; Rajapakse, S.S.; Ustin, S.L. *Remote Sensing of Environment.* **2008**, *112,* 4034-4047.

14. Goel, P.K.; Prasher, S.O.; Landry, J.A.; Patel, R.M.; Bonnell, R.B.; Viau, A.A.; Miller, J.R. *Computers and Electronics in Agriculture.* **2003**, *38,* 99-124.

15. Cremers, D. A.; Radziemski, L. J. *Handbook of Laser-Induced Breakdown Spectroscopy;* John Wiley & Sons: West Sussex, UK, 2006.

16. Singh, J. P.; Thakur, S.N. *Laser-Induced Breakdown Spectroscopy;* Elsevier: Amsterdam, Netherlands, 2007.

17. Miziolek, A. W.; Palleschi, V.; Schechter, I. *Laser-Induced Breakdown Spectroscopy (LIBS): Fundamentals and Applications;* University Press: Cambridge, UK, 2006.

18. Gamble, G.R.; Park, B.; Yoon, S.C.; Lawrence, K.C. *Applied Spectroscopy*. **2016**, *70,* 494-504.

19. Gaudiuso, R.; Dell' Aglio, M.; De Pascale, O.; Senesi, G.S.; De Giacomo, A. *Sensors*. **2010**, *10,* 7434-7468.

20. Wang, J.; Zheng, P.; Liu, H.; Fang, L. *Anal. Methods*. **2016**, *8,* 3204-3209.

21. Diaz, D.; Hahn, D. W.; Molina, A. *Applied Spectroscopy*. **2012**, *66,* 99-106.

22. Andersen, M.S.; Frydenvang, J.; Henckel, P.; Rinnan, A. *Food Control*. **2016**, *64,* 226-233.

23. Tripathi, D.K.; Singh, V.P.; Prasad, S.M.; Dubey, N.K.; Chauhan, D.K.; Rai, A.K. *Journal of Photochemistry & Photobiology, B: Biology*. **2016**, *154,* 89-98.

24. Bilge, G.; Boyaci, I.H.; Eseller, K.E.; Tamer, U.; Cakir, S. *Food Chemistry*. **2015**, *181,* 186-190.

25. Kim, G.; Kwak, J.; Choi, J.; Park, K. *J. Agric. Food Chem*. **2012**, *60,* 718-724.

26. Carvalho, G.G.A.; Moros, J.; Santos, D.; Krug, F.J.; Laserna, J.J. *Analytica Chemica Acta*. **2015**, *876,* 26-38.

27. Samek, O.; Lambert, J.; Hergenroder, R.; Liska, M.; Kaiser, J.; Novotny, K.; Kukhlevsky, S. *Laser Phys. Lett.* **2006**, *3,* 21-25.

28. Santos, D. Jr.; Nunes, L.C.; Carvalho, G.G.A.; Silva Gomes, M.; Souza, P.F.; Oliveira Leme, F.; Santos, L.G.C.; Krug, F.J. *Spectrochimica Acta Part B*. **2012**, *71-72,* 3-13,

29. Chen, H.; Li, H.; Sun, YC.; Wang, Y.; Lu, PJ. *Scientific Reports*. **2016**, *6,* 1-8.

30. Dong, Z.; Zhou, X.; Wu, J.; Zhang, Z.; Li, T.; Zhou, Z.; Zhang, S.; Li, G. *Br J Ophthalmol*. **2013**, *0,* 1-7.

31. Farjo, A.A.; Sugar, A.; Schallhorn, S.C.; Majmudar, P.A.; Tanzer, D.J.; Trattler, W.B.; Cason, J.B.; Donaldson, K.E.; Kymionis, G.D. *Ophthalmology*. **2013**, *120,* e5-e20.

32. Chen, F.; Vasquez de Aldana, J.R. *Laser Photonics Rev*. **2014**, *8,* 251-275.

33. Knudsen, K. E. *Animal Feed Science Technology*. **1997**, *67,* 319-338.

34. Herman, W. A.; McGill, W. B.; Dormaar, J. F. *Canadian Journal of Soil Sciences*. **1977**, *57,* 205-215.

35. Zhang, S.; Wang, X.; He, M.; Jiang, Y.; Zhang, B.; Hang, W.; Huang, B. *Spectrochemica Acta Part B*. **2014**, 97, 13-33.

36. Kramida, A., Ralchenko, Yu., Reader, J., and NIST ASD Team (2015). *NIST Atomic Spectra Database* (ver. 5.3), [Online]. Available: http://physics.nist.gov/asd (accessed Dec. 14, 2015).

37. Assion, A., Wollenhaupt, M., Haag, L., Mayorov, F., Sarpe-Tudoran, C., Winter, M., Kutschera, U., Baumert, T. *Appl. Phys. B* **2003**, 77, 391-397.

38. Fortes, F. J., Lasersna, J. J. *Spectrochim. Acta B* **2010**, 65, 975-990.

39. Stelmaszczyk, K., Rohwetter, P., Mejean, G., Yu, J., Salmon, E., Kasparian, J., Ackermann, R., Wolf, J.-P., and Woste, L. *Appl. Phys. Lett*. **2004**, 85, 3977.

CHAPTER FIVE

Aluminum Plasmonic Nano-Shielding in Ultraviolet Inactivation of *E. coli* Bacteria

Abstract

Ultraviolet radiation is an effective bacterial inactivation technique with broad applications in environmental disinfection. However, biomedical applications are limited due to the low selectivity, undesired inactivation of beneficial bacteria and damage of healthy tissue. New approaches are needed for the protection of biological cells and controlled treatment. Here, we investigate the effects of aluminum nanoparticles prepared by sonication of aluminum foil on the ultraviolet inactivation of *E. coli* bacteria and demonstrate a new radiation protection mechanism via plasmonic nano-shielding. We observe direct interaction of the bacterial cells with the aluminum nanoparticles and elucidate the nano-shielding mechanism via ultraviolet plasmonic resonance and nano-tailing effects. Our results provide a step towards developing improved radiation-based bacterial treatments.

Introduction

Bacterial inactivation has recently received much attention due to the rising concern of antibiotic resistance [1]. Many alternative bacterial inactivation techniques have been developed such as photodynamic [2-5] and photothermal [6,7] treatments. Ultraviolet (UV) radiation has also been used for inactivating bacteria finding many applications such as the treatment of wound infections [8,9], water [10,11] and air [12-14] disinfection and many others.

UV radiation at 254 and 280 nm inactivates bacteria by damaging DNA and proteins, respectively [14,15]. However, it does not discriminate between beneficial and pathogenic bacteria or healthy tissues. In order to develop selective bacterial UV disinfection treatments, it is necessary to improve UV protection techniques which could be used to counteract the UV inactivation for selected targets. The microparticle-based protection of fecal coliform bacteria in waste water was investigated [16]. In the former case, only a few types of bacteria have the ability to synthesize the Fe-based compounds. In the latter case, the disadvantage of the large size (> 20 μm) microparticles and low protection efficiency (< 1 %) limit the practical applications.

Here we investigate the effects of aluminum nanoparticles (Al NPs) on the UV disinfection of *E. coli* bacteria and develop a new approach to protecting bacteria from the UV radiation using plasmonic nano-shielding.

Fig. 5.1 schematically depicts the three main trials conducted utilizing *E. coli* bacteria and Al NPs and are as follows: *E. coli* bacteria exposed to UV light without the presence of Al NPs (see Figs. 5.1a and 5.1b), *E. coli* bacteria exposed to UV light with Al NPs present in the solution (see Figs. 5.1c and 5.1d), and *E. coli* bacteria exposed to UV light through UV quartz glass slide with Al NPs present on the surface of the slide (see Figs. 5.1e and 5.1f).

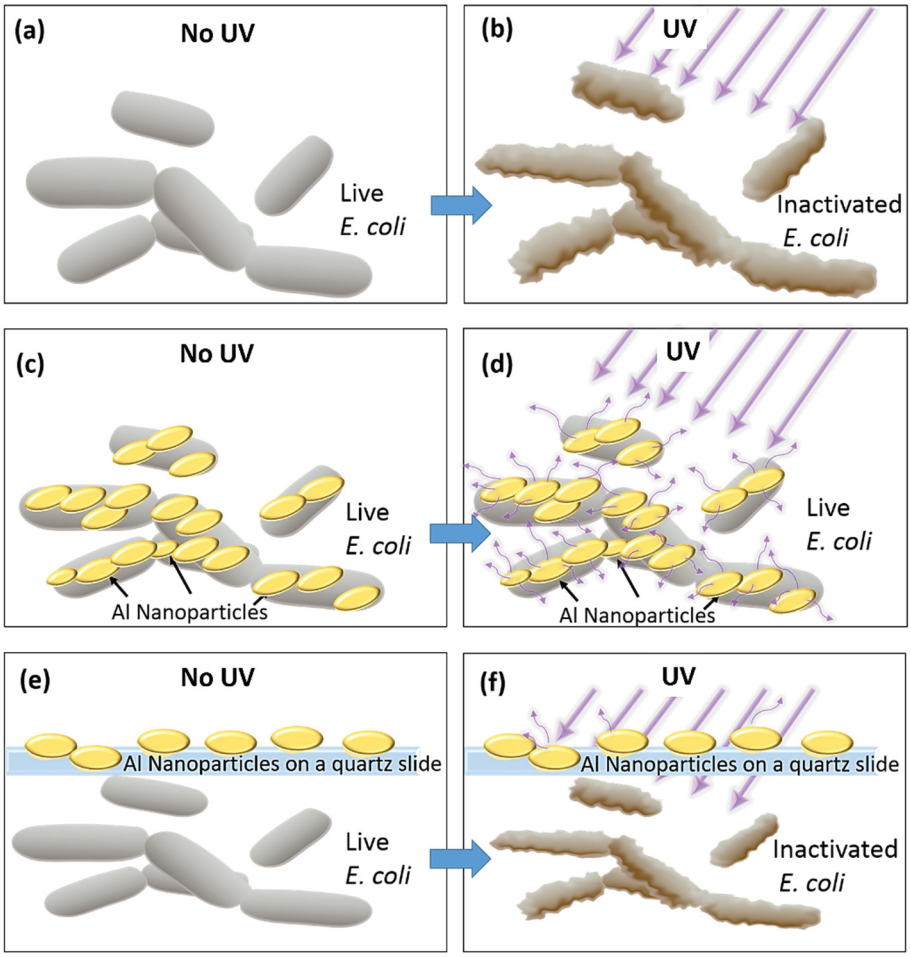

Figure 5.1. Shielding of *E. coli* bacteria from UV radiation using plasmonic aluminum nanoparticles. Schematic of the UV radiation effects on *E. coli* without (a,b) and with (c, d) Al NPs. After exposure to UV radiation, the unprotected bacteria are inactivated (b) but the protected bacteria are unharmed (d). Control experiments using a quartz slide to separate the Al NPs from bacteria show inactivation after UV irradiation (e,f).

Methods

E. coli bacteria (K-12) was obtained in slant tubes from Carolina Biological. *E. coli* was removed from the slant tubes using a sterile inoculation loop and placed in a 10 mL Lysogeny broth (LB). The broth was then placed in an incubating shaker (Fisher Scientific) at 37° C and 180 rpm for 24 hours to obtain a final concentration of ~1.5 x 10^9 colony forming units (CFU) per mL. The liquid broth culture was sealed with parafilm and stored at 4° C until use.

In a typical synthesis, 0.16 g Al foil was cut into 2 mm×2 mm pieces and put into 100 mL ethylene glycol in a Erlenmeyer flask. The mixture was put into Branson 2510 ultrasonic cleaner (Branson Ultrasonics Danbury, CT, U.S.A) for ultrasonic milling. During the ultrasonication, it was observed that Al foil gradually fragmented to smaller pieces and the color of the mixture slowly changed from a colorless to grayish black solution. After 20 hours, sonication was stopped by turning of the ultrasound; the mixture was left on the desk counter for an hour to settle. The upper layer mixture from this solution was centrifuged at 2000 RPM (Beckman Coulter Optima XPN 1000) for 10 minutes to remove bigger particles. Al nanoparticles of different sizes can be separated at 8000 RPM, 12000 RPM, 20000 RPM and 25000 RPM for 20 minutes, respectively. Al NPs were washed before adding to E. coli solution by centrifugation in DI water. DI water was added to Al NPs solution and centrifuged at a rate of 3700 rpms for 5 minutes x4. The fifth and final washing was similarly done with DI water at 3700 rpms, but for 10 minutes. Supernatant was drained and Al NPs were stored at room temperature in approximately 2 ml of DI water before addition to E. coli solution (see Figs. 5.2a and 5.2b).

The sample solution was prepared by combining 25% by volume *E. coli* liquid culture (1.5 x 10^9 CFU/ml) in LB broth with 25% Al NP solution (18.8 mg/ml); the remaining 50% of the solution was deionized water. 5 µl of the total sample solution was placed on nutrient agar in a petri dish and circularly spread to a diameter of approximately 1.5 cm using a sterilized spatula. The sample was then placed in the beam path of a Xenon lamp (Spectral Products, ASB-XE-175) using a monochromator (Spectral Products, CM110) to select the desired UV spectral range. Illumination was

performed for 5, 10, 20, and 30 minutes resulting in the UV doses of 9, 18, 36 and 54 mJ/cm^2, respectively. The samples were then incubated at 37^o C for 24 hours. Each set of measurements was repeated six to eight times with qualitatively similar results.

For the scanning electron microscopy (SEM) measurements, the *E. coli* bacterial cells (with and without nanoparticles) were fixed with 2.5% glutaraldehyde in 0.06 M phosphate buffer (pH 7.2) for 90 minutes at room temperature and then washed 4 times 10 minutes each in the buffer solution. The samples were then dehydrated using a graded series of ethanol for 2 times 10 minutes at each step (50%, 70%, 90%, and 100%). After critical point drying (EM CPD300, Leica Microsystems, Wetzlar, Germany) samples were mounted on stubs and sputter coated (EM ACE 600, Leica Microsystems) with approximately 15 nm of carbon. SEM measurements were performed in a Versa 3D scanning electron microscope (FEI, Hillsboro, OR, USA). Energy-dispersive X-ray spectroscopy (EDS) was performed with an Octane Pro Silicon Drift Detector (EDAX, Mahawah, NJ, USA) at 20 KV, spot size 7, and at a working distance of 10 mm.

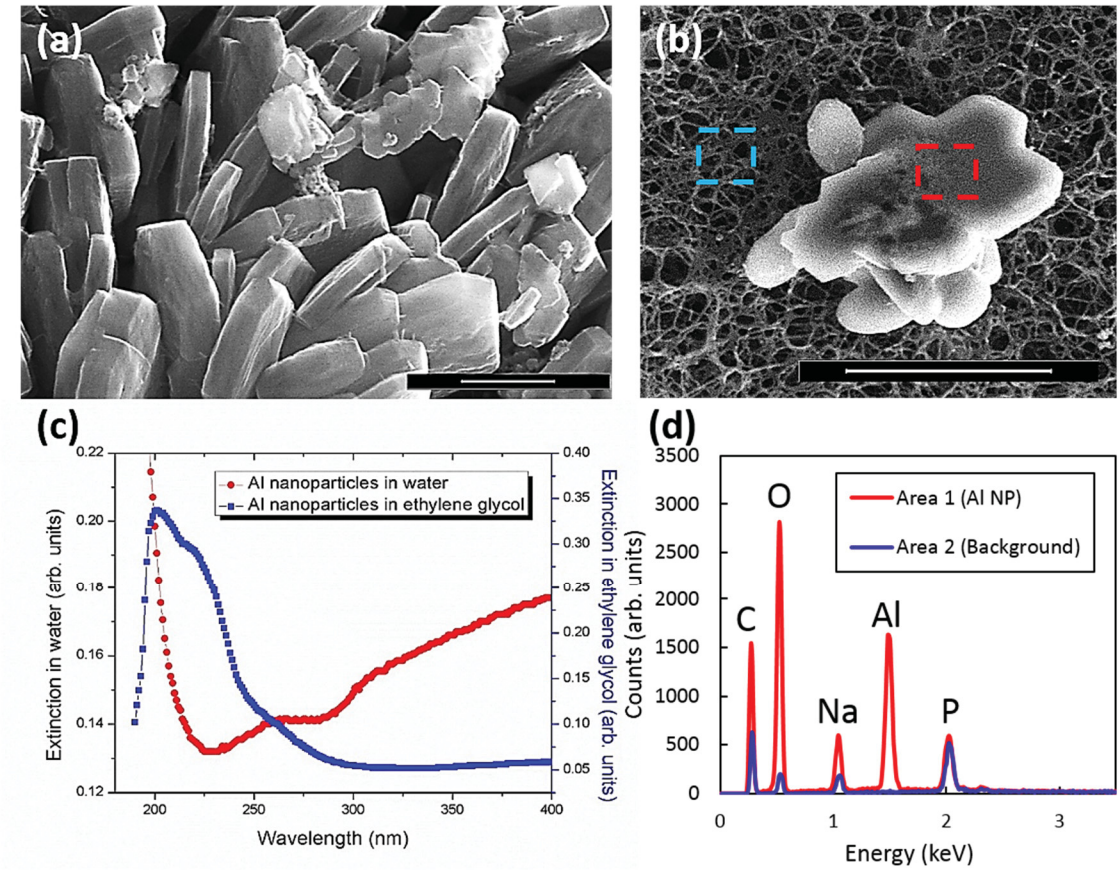

Figure 5.2 Characterization of E. coli bacteria shielded by aluminum nanoparticles. SEM images of the Al NPs (a) and of E. coli bacteria shielded by Al NPs (b). (c) Extinction spectra of Al NPs in water (red circles) and in ethylene glycol (blue squares). (d) EDS spectra of E. coli bacteria shielded by Al NPs obtained from the areas on the Al NP (red) an on the substrate (blue) corresponding to the highlighted dashed red and blue areas in (b), respectively. The scale bar is 500 nm in (a) and 2 μm in (b).

Results

SEM images show typical structures of Al NPs (Fig. 5.2a) and *E. coli* shielded by Al NPs (Fig. 5.2b). EDS analysis was performed to confirm the elemental composition of the Al NPs attached to the bacteria. Fig. 2d shows the presence of the Al and O elements in the nanoparticle-bacteria aggregate (corresponding to the red dashed square in Fig. 5.2b) and the absence on the substrate (corresponding to the blue dashed square in Fig. 5.2b).

The nano-shielding effect is revealed in the bacterial viability measurements shown in Fig. 5.3. Figure 5.3a shows no significant *E. coli* colony formation after the 54 mJ/cm^2 UV radiation without Al NPs. However, with the addition of Al NPs, a fraction of *E. coli* bacteria were still able to thrive and form colonies after incubation. Figure 5.3 shows data from a single petri dish with two separate irradiated sample areas highlighted by red circles. UV dose dependence for inactivation of *E. coli* with and without Al NPs is shown in Fig. 5.3c.

We also performed control measurements under the same conditions with the same concentration of Al NPs placed on a quartz slide separating Al NPs and *E. coli* and exposed to UV radiation as schematically shown in Figs. 1e and 1f. Nearly all *E. coli* were inactivated (not shown) regardless of the presence of Al NPs similar to the results without NPs shown in Fig. 5.3a. These control results, in conjunction with the results showing that Al NPs preserved *E. coli* CFUs in contact with nanoparticles imply that the shielding effect is due to the direct interaction of *E. coli* with Al NPs.

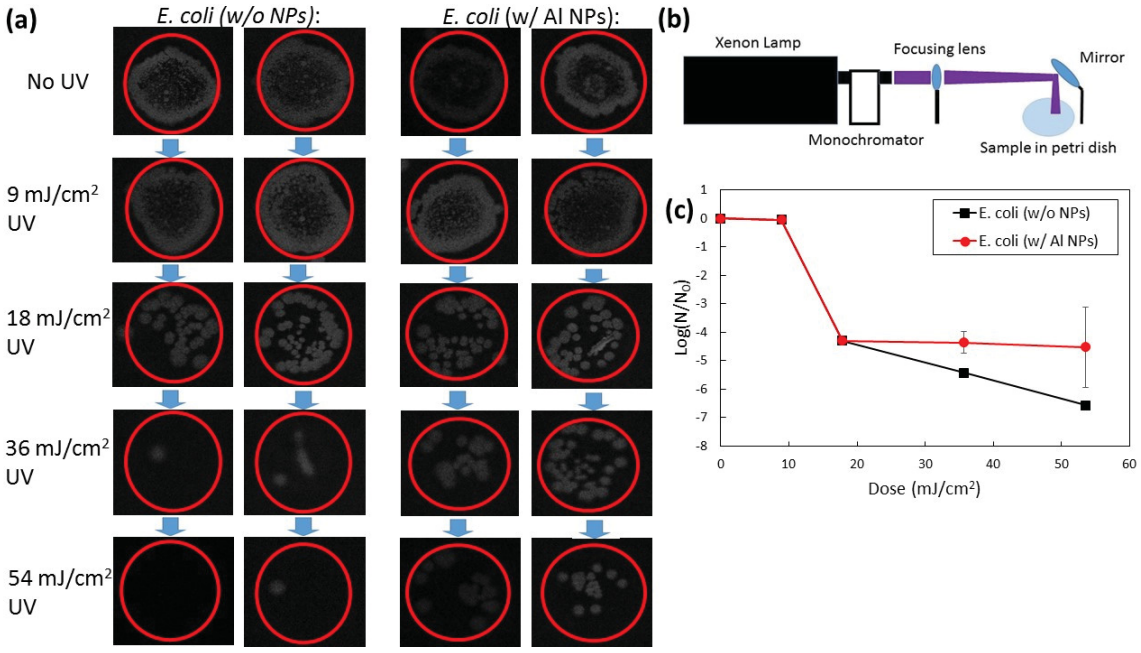

Figure 5.3. Nano-shielding effects in UV inactivation of E. coli bacteria. (a) Photographic images showing the culture growth of E. coli bacteria after exposure to 0, 9, 18, 36 and 54 mJ/cm2 dose of UV radiation at 254 nm with and without Al NPs. (b) Schematic of the experimental setup. (c) UV dose dependence of *E. coli* survival Log(N/N0) with and without Al NPs.

The concentration dependence of Al NPs and *E. coli* is shown in Figs. 4a and 4b, respectively. As the Al NP concentration is increased, the shielding of *E. coli* bacteria from the damaging UV radiation has an upward trend (i.e. more CFUs are conserved, see Fig. 5.4a). The addition of increasing concentrations of Al NPs without exposure to UV radiation shows very little change in the number of viable CFUs; therefore, Al NPs themselves do not show any toxic effects on the *E. coli*.

The wavelength dependence of the UV radiation effects is shown in Figs. 5.4c and 5.4d. Figure 5.4c shows that without Al NPs both the 254 nm and 280 nm radiation was able to inactivate *E. coli*. In comparison, irradiation at 300 nm and 350 nm under identical conditions did not have any significant effect. When 25% of Al NPs were used, the inactivation of *E. coli* was suppressed at all wavelengths (Fig. 5.4d).

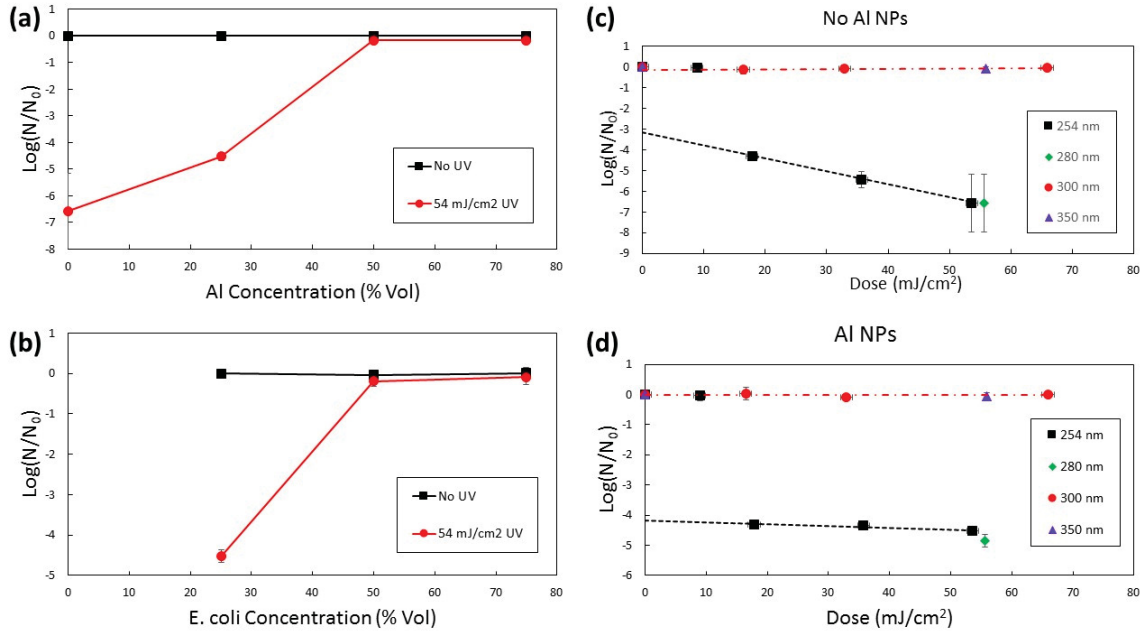

Figure 5.4. Concentration and wavelength dependence of bacterial inactivation. *E. coli* inactivation with varying concentration of Al NPs (a) and *E. coli* (b). Wavelength dependence of E. coli inactivation without (c) and with (d) Al NPs.

Discussion

Numerous physical and chemical methods have been developed to inactivate bacteria [6-8,16-18]. Au and Ag NPs with a variety of sizes and shapes have been shown as effective anti-bacterial metallic nanoparticles due to their plasmonic resonances in the visible and NIR ranges resulting in the enhanced photothermal and photodynamic effects [7,19,20]. However, to the best of our knowledge, no reports of shielding behavior using Ag or Al plasmonic nanoparticles have been made. On the other hand, Au NPs with certain sizes form aggregates with varying photodynamic activities due to their light scattering and/or shielding effects [21]. These techniques mentioned focus on utilizing the visible regime of the spectrum. However, another photo-inactivation method is the use of UV radiation, which damages DNA and proteins of both desirable and undesirable microorganisms. Because of this, we seek to protect bacteria from UV radiation as a first

step to developing new approaches for the controlled inactivation of bacteria. Here we show that Al NPs interact with *E. coli* to form aggregates that shield the bacteria from the harmful UV radiation.

Because *E. coli* bacterial cells have a negative surface charge on the outer membrane [22,23], they can electrostatically attach to metallic nanoparticles. Since the Al plasmonic nanoparticles are efficient light absorbers and scatterers in the UVC regime (see Fig. 5.2c), this works as a nanoscale mirror or attenuator, thus shielding the attached bacteria from the damaging UV radiation (see Figs. 5.1 and 5.3). We observed shielding capabilities in Al nanoparticle aggregates as small as 2 μm in size (see Fig. 5.2b); whereas, other reports of shielding from non-plasmonic materials were on the order of 20 μm and above [16]. This enhanced shielding proficiency may be due to the plasmonic resonances in the UV regime which leads to an enhanced extinction cross section. Additionally, the light scattering properties of the Al NPs are enhanced by the shape of the nanoparticle produced by the method detailed above [20].

Typical cell survival curves for cells exposed to ionizing radiation can be modeled using either the multi-target or linear-quadratic model [24]. Both of these models exhibit a shoulder region, characterized by an initial gently sloping section, followed by a region of steeper decent. Our data follow this trend; however, with the addition of the Al NPs to the *E. coli* solution before exposure to UV light, the slope of the second region has been substantially reduced (see Figs. 5.4c and 5.4d). Fractionation of the total dose could possibly provide further reduction of the slope.

Acknowledgements

This work was supported by the National Science Foundation under Grants CHE-1609608 and PHY-1307153, the Office of Naval Research grant N00014-16-1-3054, and the Robert A. Welch Foundation under Awards A-1261 and A-1547. We thank Prof. Touradj Solouki for helpful discussions.

References

1. CDC. Antibiotic Resistance Threats in the United States, 2013. U.S. Department of Health and Human Services, CDC, 2016.

2. Chen, J., Cesario, T.C. & Rentzepis, P.M. Rationale and mechanism for the low photoinactivation rate of bacteria in plasma. *PNAS* **111**, 33-38 (2014).

3. Vantansever, F., Melo, W.C.M.A., Avci, P., Vecchio, D., Sadasivam, M., Gupta, A., Chandran, R., Karimi, M., Parizotto, N.A., Yim, R., Tegos, G.P. & Hamblin, M.R. Antimicrobial strategies centered around reactive oxygen species-bacterial antibiotics, photodynamic therapy, and beyond. *FEMS Microbial Rev* **37**, 955-989 (2013).

4. Wu, J., Xu, H., Tang, W., Kopelman, R., Philbert, M.A. & Xi, C. Eradication of bacteria in suspension and biofilms using methylene blue-loaded dynamic nanoplatforms. *Antimicrob. Agents Chemother.* **53**, 3042-3048 (2009).

5. Simon, T., Boca-Farcau, S., Gabudean, A.M., Baldeck, P. & Astilean, S. LED-activated methylene blue-loaded Pluronic-nanogold hybrids for *in vitro* photodynamic therapy. *J. Biophotonics* **6**, 950-959 (2013).

6. Zharov, V.P., Mercer, K.E., Galitovskaya, E.N. & Smeltzer, M.S. Photothermal nanotherapeutics and nanodiagnostics for S\selective killing of bacteria targeted with gold nanoparticles. *Biophysical Journal* **90**, 619-627 (2006).

7. Santos, G.M., Ferrara, F.I.S. Zhao, F., Rodrigues, D.F. & Shih, W.C. Photothermal inactivation of heat-resistant bacteria on nanoporous gold disk arrays. *Optical Materials Express* **6**, 1217-1229 (2016).

8. Dai, T., Vrahas, M.S., Murry, C.K. & Hamblin, M.R. Ultraviolet C irradiation: an alternative antimicrobial approach to localized infections? *Expert Review of Anti-Infective Therapy* **10**, 185—95 (2012).

9. Gupta, A., Avci, P., Dai, T., Huang, Y.Y. & Hamblin, M.R. Ultraviolet radiation in wound care: sterilization and stimulation. *Advances in Wound Care* **2**, 422-437 (2012).

10. Meulemans, C.C.E. The basic principles of UV-disinfection of water. *Ozone: Science & Engineering* **9**, 299-313 (1986).

11. Wolfe, R.L. Ultraviolet disinfection of potable water. *Environ. Sci. Technol.* **24**, 768-773 (1990).

12. Ko, G., First, M.W. & Burge, H.A. The characterization of upper-room ultraviolet germicidal irradiation in inactivating airborne microorganisms. *Environmental Health Perspectives* **110***,* 95-101 (2002).

13. Reed, N.G. The history of ultraviolet germicidal irradiation for air disinfection. *Public Health Reports* **125**, 15-27 (2010).

14. *Kowalski W.J., Bahnfleth W.P., Witham D.L., Severin B.F. & Whittam T.S.* Mathematical modeling of ultraviolet germicidal irradiation for air disinfection*. Quantitative Microbiology **2,** 249–270 (2000).*

15. Chang, J.C.H., Ossoff, S.F., Lobe, D.C., Dorman, M.H., Dumais, C.M., Qualls, R.G. & Johnson, J.D. UV inactivation of pathogenic and indicator microorganisms. *Applied and Environmental Microbiology* **49**, 1361-1365 (1985).

16. Madge, B.A. & Jensen, J.N. Ultraviolet disinfection of fecal coliform in municipal wastewater: effects of particle size. *Water Environment Research* **78**, 294-304 (2004).

17. El-Azizi, M. & Khardori, N. Efficacy of ultraviolet C light at sublethal dose in combination with antistaphylococcal antibiotics to disinfect catheter biofilms of methicillin-susceptible and methicillin-resistant Staphylococcus aureus and Staphylococcus epidermis in vitro. *Infection and Drug Resistance* **9**, 181-189 (2016).

18. Dean, S.J., Petty, A., Swift, S., McGhee, J.J., Sharma, A., Shah, S. & Craig, J.P. Efficacy and safety assessment of a novel ultraviolet C device for treating corneal bacterial infections. *Clinical and Experimental Ophthalmology* **39**, 156-163 (2011).

19. Castillo-Martinez, J.C., Martinez-Castanon, G.A., Martinez-Gutierrez, F., Zavala-Alonso, N.V., Patino-Marin, N., Nino-Martinez, N., Zaragoza-Magana, V. & Cabral-Romero, C. Antibacterial and antibiofilm activities of the photothermal therapy using gold nanorods against seven different bacterial strains. *Journal of Nanomaterials* **2015**, 1-7 (2015).

20. Austin, L.A., Mackey, M.A., Dreaden, E.C. & El-Sayed, M.A. The optical, photothermal, and facile surface chemical properties of gold and silver nanoparticles in biodiagnostics, therapy, and drug delivery. *Arch. Toxicol.* **88**, 1391-1417 (2014).

21. Perni, S., Piccirillo, C., Kafizas, A., Uppal, M., Prattan, J., Wilson, M. & Parkin, I.P. Antibacterial activity of light-activated silicone containing methylene blue and gold nanoparticles of different sizes. *J. Clust. Sci.* **21**, 427-438 (2010).

22. Pidhatika, B., Moller, J., Benetti, E.M., Konradi, R., Rakhmatullina, E., Muhlebach, A., Zimmermann, R., Werner, C., Vogel, V. & Textor, M. The role of the interplay between polymer architecture and bacterial surface properties on microbial adhesion to polyazoline-based thin films*. Biomaterials **31**, 9462-9472 (2010).*

23. Liu, L., Xu, K., Wang, H., Tan, J.P.K., Fan, W., Venkatraman, S.S., Li, L. & Yang, Y.Y. Self-assembled cationic peptide nanoparticles as an efficient antimicrobial agent. *Nature Nanotechnology **4**, 457-463 (2009).*

24. Hall, E.J. & Giaccia, A.J. Radiobiology for the Radiologist. Lippincott Williams & Wilkins (Philidelphia, PA, 2006).

CHAPTER SIX

Conclusion

LIBS for Plant Stress Detection

Stress within a plant is any unfavorable conditions or substances which negatively affects or inhibits the plant's metabolism and may be short-term or long-term [90]. Plants react differently to stress events depending upon which stress response phase. Certain stress effects can be partially offset for by acclaimation, adaptation and repair mechanisms for minor or accute stress. Chronic or strong stress can cause irreversible damage or may lead to death of the plant [90]. On a small scale, visual inspection of crops may be performed to determine the overall health of field crops. However, for large areas of vegetation, visual inspection is time consuming and sometimes impractical [10, 12, 91]. The LIBS approach has many advantages for rapid detection of plant stress that allow for this technique to be expanded to the field scale. LIBS can be performed on whole plants without any sample preparation. Additionally, LIBS requires few optical components. Because of these key features, LIBS has the potential to be performed remotely via drone/UAV, allowing for rapid monitoring of vast crop terrain.

Due to the relative simplicity of the method and the ability to monitor elemental contents in plants on the laboratory and field scales, LIBS has the potential to offer insights into the complex mechanisms of plant tolerance and stess response such as the relative K and Na level dynamics, Ca accumulation and transport, and many others. Optimal K^+/Na^+ ratio is crucial for plant metabolism and plays an important role in the osmotic adjustment and stress tolerance under drought and salinity [8, 92]. For example,

a significant increase of K^+ and Na^+ was reported under drought [93, 94, 95]. High tolerance to the combined drought and salinity stress was previously related to the lower Na^+/K^+ ratio [96]. Our results indicate an increase in the relative content Na/K ratio in wheat. Drought and salinity can also affect Ca2+ content [4, 95, 97]. Further, water deprivation has been shown to damage the mechanism controlling Fe uptake which leads to increased Fe concentraiton in the chloroplasts [98]. LIBS may provide a better understanding of the role of these ions in the stress response. Although the LIBS technique is realtively simple, the interperpation of the data can be complex due to the many factors that effect the sample matrix and plasma conditions. Therefore, the observed LIBS signals are due to the contributions of the changing elemental contents and to the changes in the sample matrix brought about by the induced drought stress. Both factors may be considered as signatures of the drought stress and may be used for the rapid detection of stress in plants.

Our experimental implimentation of LIBS can be further improved by optimizing several parameters such as the lens-to-sample (LTS) distance which plays a minor role for long focal length lenses due to the gradual nature of the focus and increase in the focal volume [13]. Therefore, the LTS can be optimized for stand-off field applications. The detector sensitivity and spectral efficiency are additional control parameters which determine the effectiveness of LIBS in monitoring plant stress. Higher resolution detectors are useful for deconvoluting overlaping atomic species in the LIBS spectra and may provide more precise measurements. Moreover, high resolution detectors allow for monitoring of a larger number of atomic species. LIBS signal strength can be increased using detectors with greater sensitivity and better collection efficiency over large

distances or in the presence of background. The benefits of the improved resolution and sensitivity must be balanced with the augmented size and cost of the detector in order to maintain feasability of field applications. Here we used a lightweight inexpensive spectrometer (OceanOptics HR2000) which is suitable for the use on a UAV. For comparison, we also performed LIBS measurements using a high resolution spectrometer (IsoPlane, Princeton Instruments) and obtained similar results (not shown). In addition to compact spectrometers, compact femtosecond lasers are also available which are suitable for UAV use; however, they are limited in power output. More powerful lasers can be used to increase the signal strength of LIBS or to generate femtosecond plasma filaments which can be used for filament-induced breakdown spectroscopy (FIBS) [38]. FIBS may provide similar information as LIBS with the advantage of longer standoff detection range. Field-scale filament-based environmental analysis was previously performed on a vehicle platform (TERAMOBIL) [99]. It is envisioned that similar technology may be developed for agricultural applications.

In addition to the monitoring of drought stress, the LIBS method can be expanded to include elemental signals of other types of stress and to include other economically meaningful plant species. LIBS may be performed on a large scale in different environments and may be used for comparative field studies between different countries [100]. LIBS may be used to determine spectroscopic signatures of a plethora of stressors for different crops, thereby allowing for greater understanding of the mechanisms of, and improved response to, stress factors found in plant life.

LIBS for Distinguishing Between Crops and Weeds

LIBS is a functional technique with many advantages, especially for remote field observations. Here we present a simple method that can distinguish between various plant species, with practical applications for identifying and differentiating crops and weed species. Because most plants share several common elements and compounds, the peaks that appear in the typical LIBS spectra are very similar [see Figure 4.2]. Several modifications can be made to enhance sensitivity and improve the detection limits. One such improvement is that of a higher resolution detector. An addition, using a detector with an extended spectral range would allow for the possibility of collecting and observing other Ca I lines providing more data points for the Boltzmann plots and therefore increasing precision in plasma temperature calculations [55]. Though these advantages are compelling, one must weigh these benefits against the increased cost and decreased mobility that accompany enhanced detectors. Along with the increased spectral region of the detector, a notch filter in place of the color glass filter in order to suppress the back-scattered laser radiation would provide an extra improvement in resolution and sensitivity and would allow for detecting additional elements in a broader spectral range.

Further improvements could be achieved by varying the temporal width of the laser pulses. Most LIBS approaches used ns laser pulses for the analysis of plant materials. For example, using the ns LIBS could reduce the cost of the laser system and achieve pulses with energies on the order of a few hundred mJ which may generate hotter plasma with more detectable elements in the plant material. This would require using detectors with a time delay to suppress the continuum background which was shown to be lower for fs LIBS [47]. Another advantage of fs LIBS is the higher spatial resolution

due to the shorter interaction time, lower laser fluence, reduced plasma temperature and the corresponding decrease of the ablation volume [19, 78]. Also both ns and fs LIBS can be used for short-range (up to ~ 100 m) stand-off detection using telescopes [101]. However, fs laser pulses may be used for the generation of laser filaments which are advantageous for long-range (> 100 m) stand-off filament-induced laser breakdown spectroscopy [73].

Additional modifications could be made to use longer delay times between the formation of plasma and LIBS measurements. The plasma temperature at zero delay time may reach high values up to tens of thousands degrees and decrease at longer times. For simplicity we used the zero delay. Our results may be further improved by adding a longer delay time [55].

With the ability to distinguish between plants that look similar, and especially from a distance, growers and crop consultants can effectively scout for the presence of weeds in large production areas within a short time and apply herbicides to specific areas where required, allowing for a reduction in herbicide use and associated environmental impacts and improved profitability.

UV Treatment of E. coli Bacteria with Al Nanoparticles

Numerous physical and chemical methods have been developed to inactivate bacteria [61, 62, 63, 71, 102, 89]. Au and Ag NPs with a variety of sizes and shapes have been shown as effective anti-bacterial metallic nanoparticles due to their plasmonic resonances in the visible and NIR ranges resulting in the enhanced photothermal and photodynamic effects [62, 103, 104]. However, to the best of our knowledge, no reports of shielding behavior using Ag or Al plasmonic nanoparticles have been made. On the

other hand, Au NPs with certain sizes form aggregates with varying photodynamic activities due to their light scattering and/or shielding effects [105]. These techniques mentioned focus on utilizing the visible regime of the spectrum. However, another photo-inactivation method is the use of UV radiation, which damages DNA and proteins of both desirable and undesirable microorganisms. Because of this, we seek to protect bacteria from UV radiation as a first step to developing new approaches for the controlled inactivation of bacteria. Here we show that Al NPs interact with *E. coli* to form aggregates that shield the bacteria from the harmful UV radiation.

Because *E. coli* bacterial cells have a negative surface charge on the outer membrane [106, 107], they can electrostatically attach to metallic nanoparticles. Since the Al plasmonic nanoparticles are efficient light absorbers and scatterers in the UVC regime (see Fig. 5.2c), this works as a nanoscale mirror or attenuator, thus shielding the attached bacteria from the damaging UV radiation (see Figs. 5.1 and 5.3). We observed shielding capabilities in Al nanoparticle aggregates as small as 2 μm in size (see Fig. 5.2b); whereas, other reports of shielding from non-plasmonic materials were on the order of 20 μm and above [16]. This enhanced shielding proficiency may be due to the plasmonic resonances in the UV regime which leads to an enhanced extinction cross section. Additionally, the light scattering properties of the Al NPs are enhanced by the shape of the nanoparticle produced by the method detailed above [104].

Typical cell survival curves for cells exposed to ionizing radiation can be modeled using either the multi-target or linear-quadratic model [108]. Both of these models exhibit a shoulder region, characterized by an initial gently sloping section, followed by a region of steeper decent. Our data follow this trend; however, with the addition of the Al NPs to

the *E. coli* solution before exposure to UV light, the slope of the second region has been substantially reduced (see Figs. 5.4c and 5.4d). Fractionation of the total dose could possibly provide further reduction of the slope.

APPENDIX

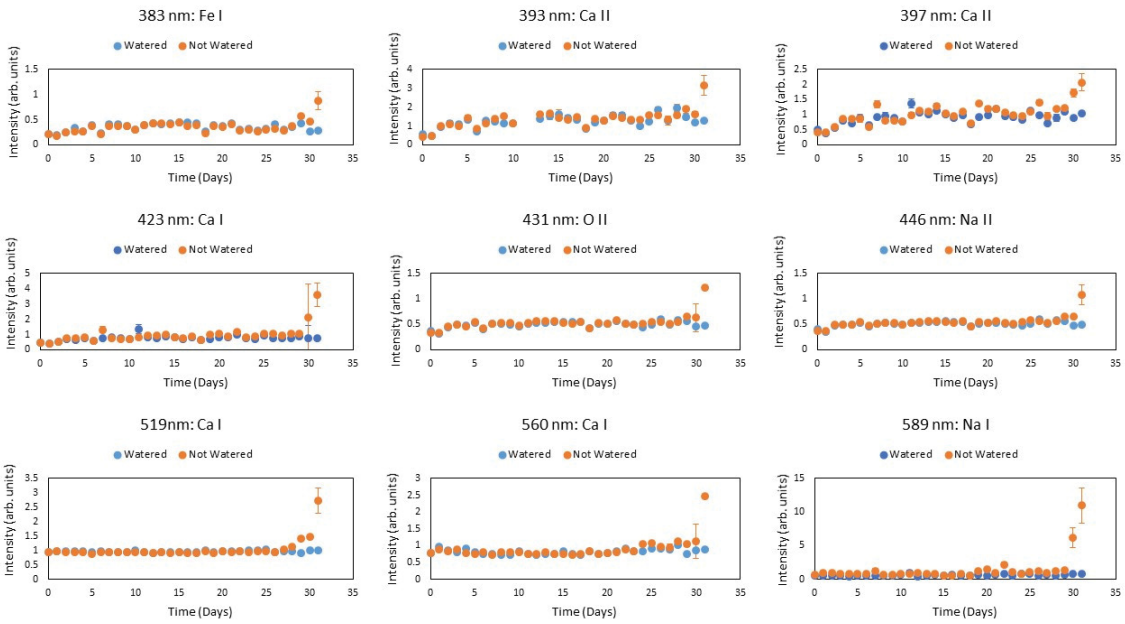

Figure A.1. Temporal evolution of average peak intensities for the observed LIBS signals from the first set of gardenia plants.

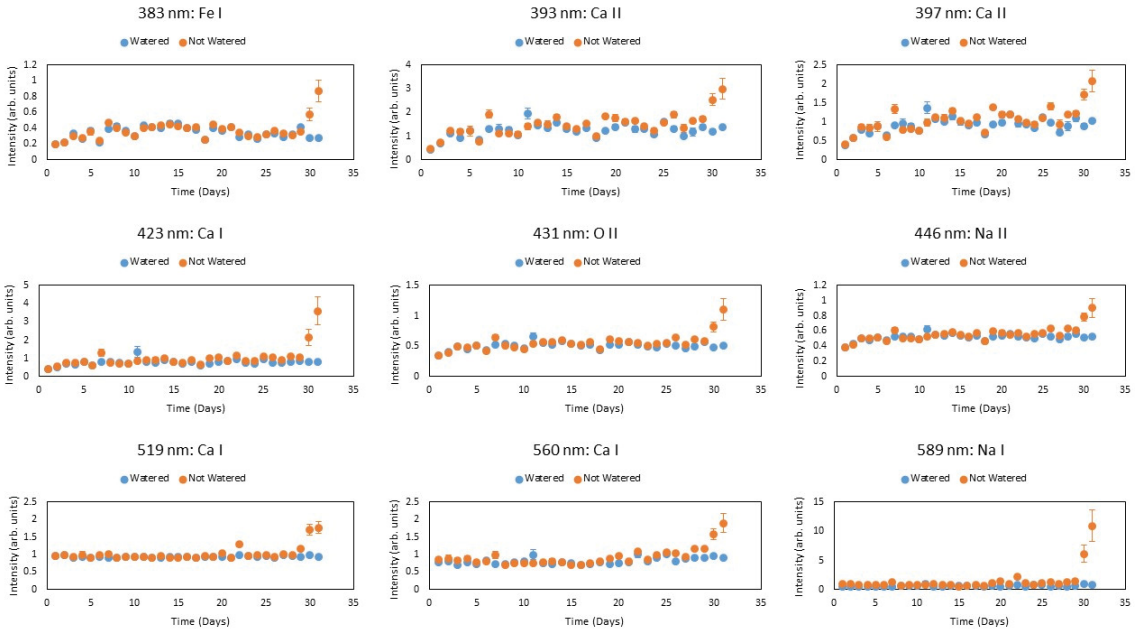

Figure A.2. Temporal evolution of average peak intensities for the observed LIBS signals from the second set of gardenia plants.

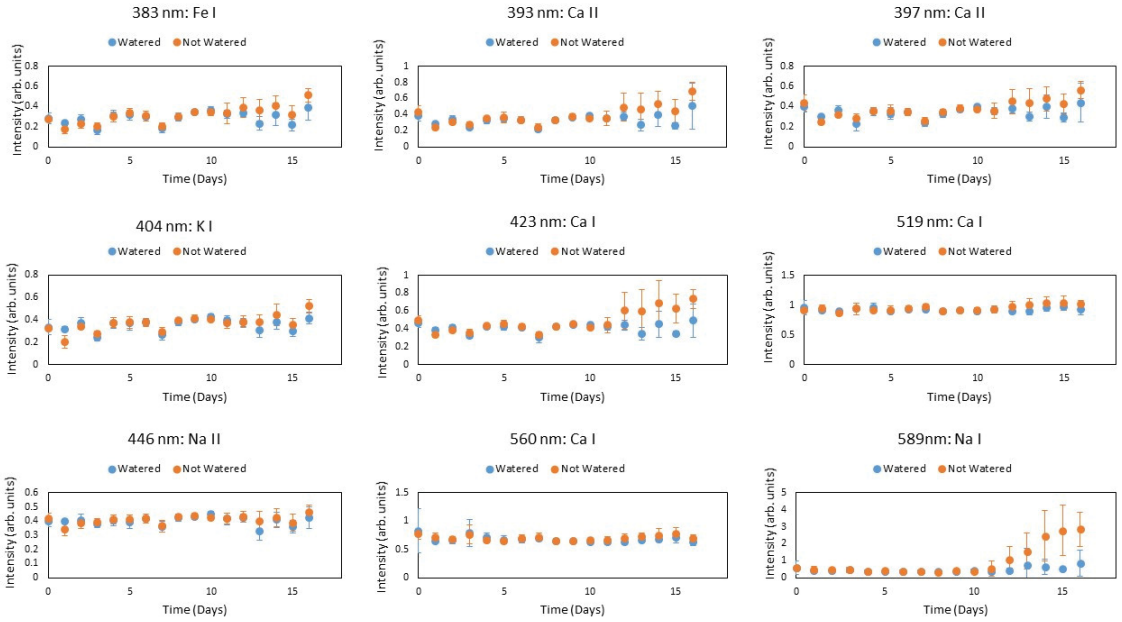

Figure A.3. Temporal evolution of average peak intensities for the observed LIBS signals from the wheat plants.

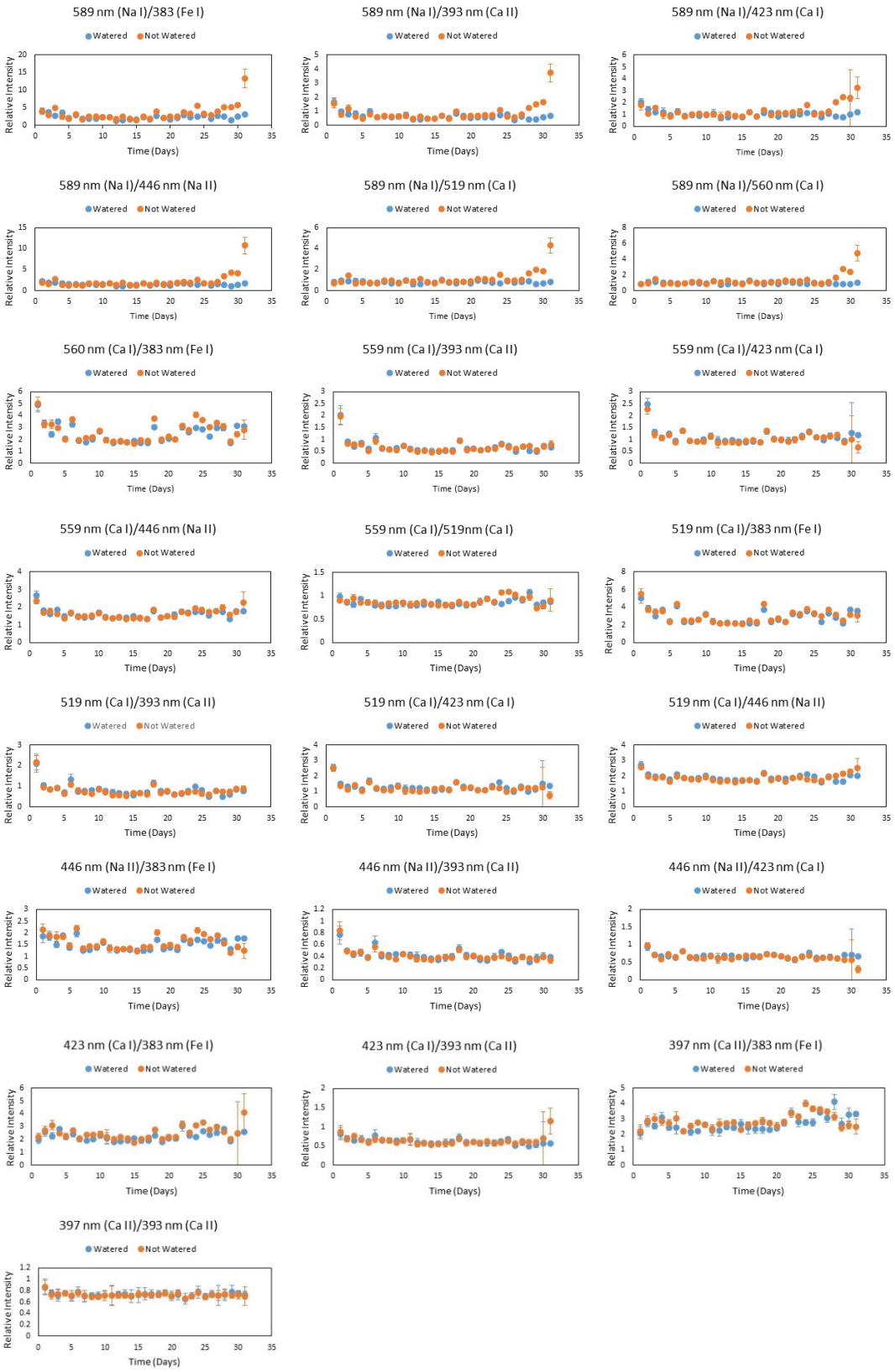

Figure A.4. Temporal evolution of peak ratios for the observed LIBS signals from the first set of gardenia plants.

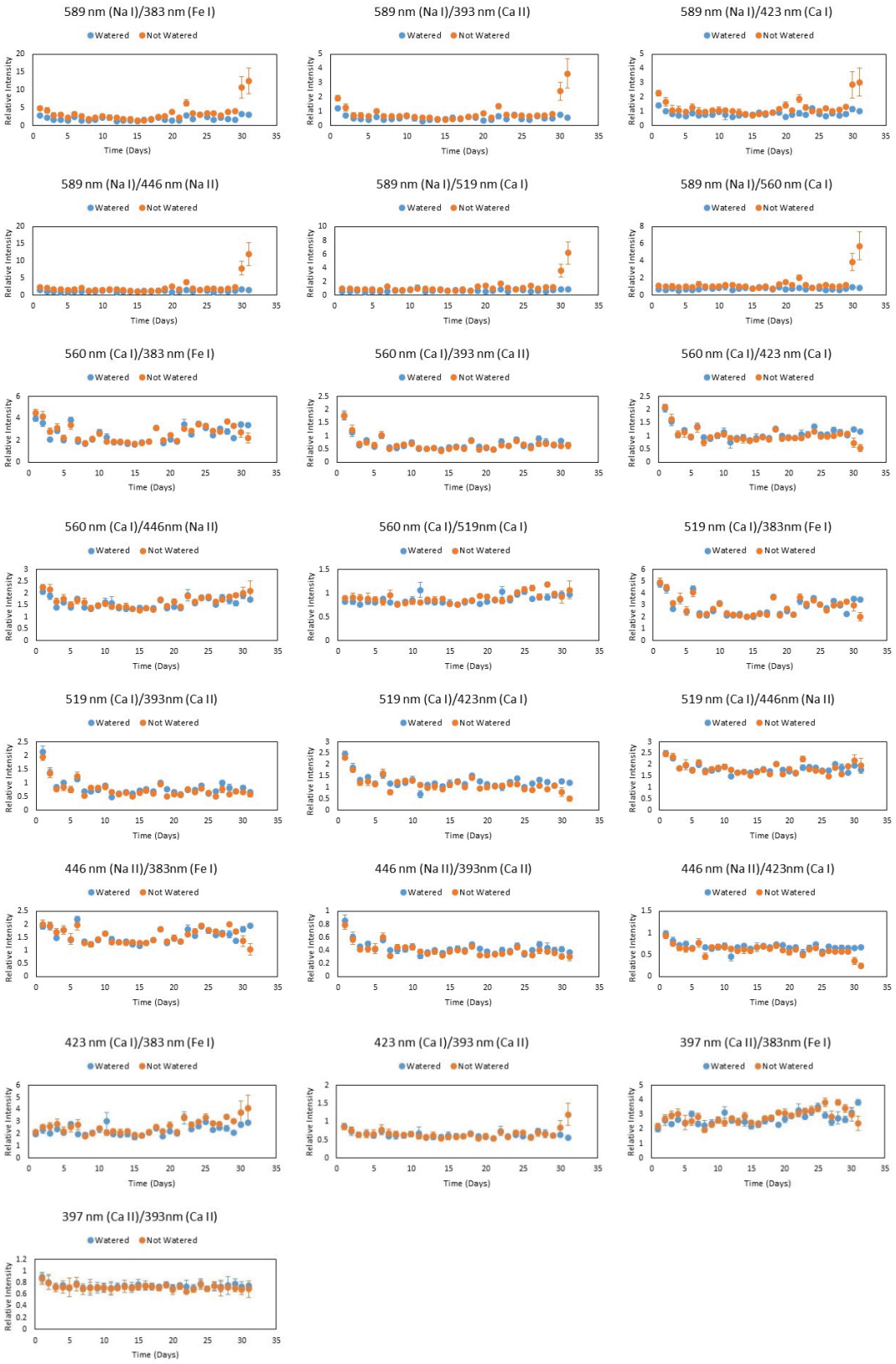

Figure A.5. Temporal evolution of peak ratios for the observed LIBS signals from the second set of gardenia plants.

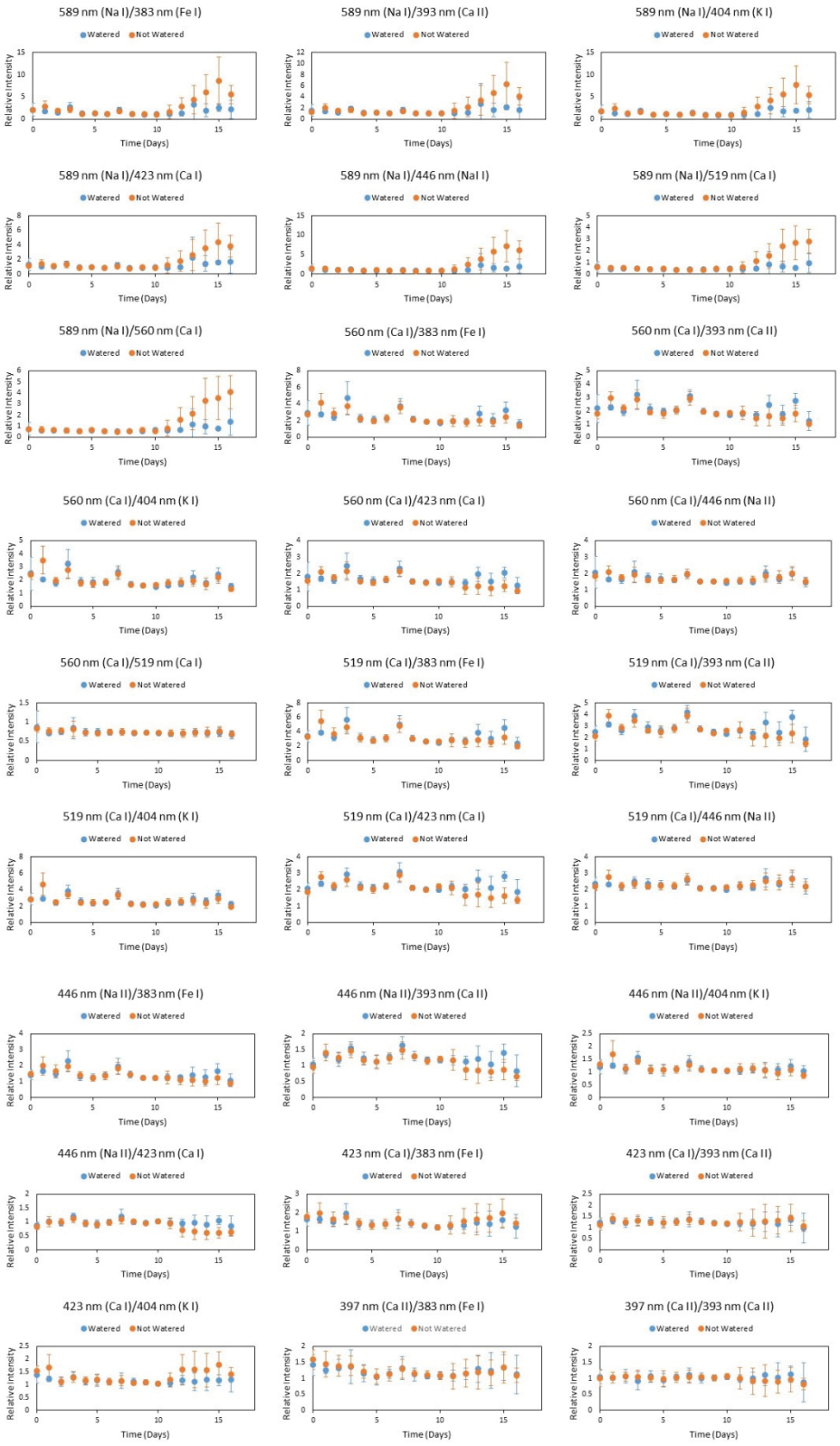

Figure A.6. Temporal evolution of peak ratios for the observed LIBS signals from the wheat plants.

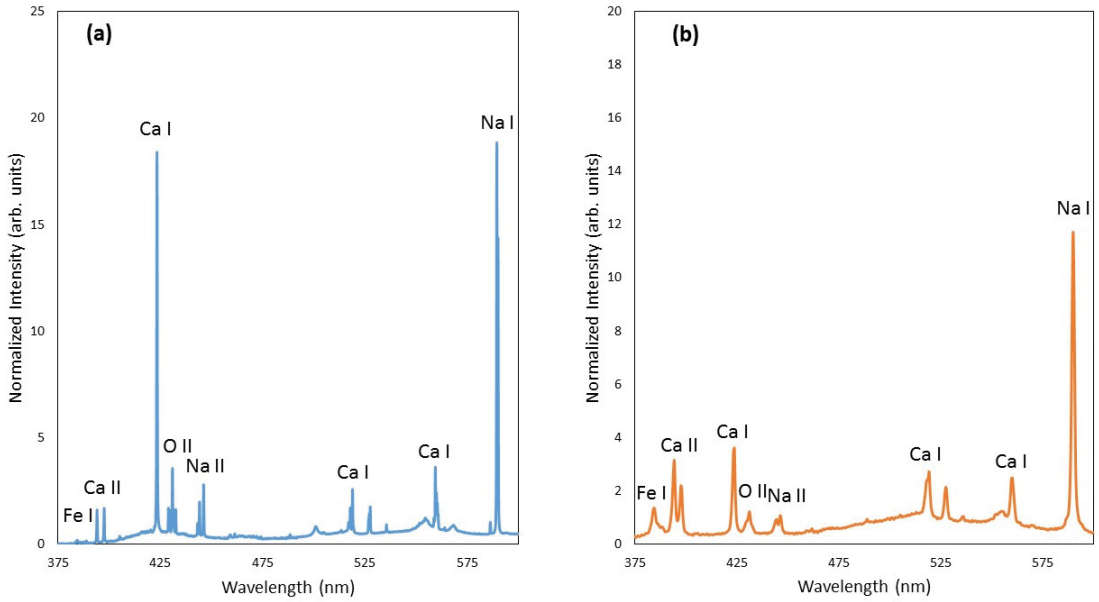

Figure A.7. LIBS spectra, with peak assignments, from a high resolution table-top spectrometer [Princeton Instruments IsoPlane SCT320 with Pixis 400b CCD camera] (a), and a lower resolution hand-held spectrometer [Ocean Optics HR2000] (b).

BIBLIOGRAPHY

[1] V. Vassileva, D. Demirevska, L. Simova-Stoilova, T. Petrova, N. Tsenov and U. Feller, "Long-Term Field Drought Affects Leaf Protein Pattern and Chloroplast Ultrastructure of Winter Wheat in a Cultivar-Specific Manner," *J. Agronomy & Crop Science,* no. 198, pp. 104-117, 2012.

[2] H. Koyro, P. Ahmad and N. Geissler, "Abiotic stress responses in plants: an overview," in *Environmental Adaptations and Stress Tolerance of Plants in the Era of Climate Change*, P. A. a. M. N. Prasad, Ed., Springer, 2012, pp. 1-28.

[3] M. Farooq, M. Hussain, A. Wahid and K. Siddique, "Drought stress in plants: an overview," in *Plant Responses to Drought Stress*, R. Aroca, Ed., Springer, 2012, pp. 1-35.

[4] S. Gill, N. Anjum, R. Gill and N. Tuteja, "Abiotic stress signaling in plants – an overview," in *Abiotic Stress Response in Plants*, N. T. a. S. S. Gill, Ed., Wiley, 2016, pp. 3-12.

[5] L. Chaerle, W. Van Caeneghem, E. Messens, H. Lambers, M. Van Montagu and D. Van Der Straeten, "Presymptomatic visualization of plant–virus interactions by thermography," *Nature Biotechnology,* vol. 17, pp. 813-816, 1999.

[6] H. Jones, "Use of thermography for quantitative studies of spatial and temporal variation of stomatal conductance over leaf surfaces," *Plant, Cell and Environment,* vol. 22, pp. 1043-1055, 1999.

[7] J. Peñuelas and I. Filella, "Visible and nearinfrared reflectance techniques for diagnosing plant physiological status," *Trends Plant Sci.,* vol. 3, pp. 151-156, 1998.

[8] J. Casanova, S. O'Shaughnessy, S. Evett and C. Rush, "Development of a wireless computer vision instrument to detect biotic stress in wheat," *Sensors,* vol. 14, p. 11153, 2014.

[9] K. Hancke, B. Sorell, L. Lund-Hansen, M. Larsen, T. Hancke and R. Glud, "Effects of temperature and irradiance on a benthic microalgal community: A combined two-dimensional oxygen and fluorescence imaging approach," *Limnol. Oceanogr.,* vol. 5, pp. 1599-1611, 2014.

[10] H. Lichtenthaler and F. Babani, "Detection of photosynthetic activity and water stress by imaging the red chlorophyll fluorescence," *Plant Physiol. Biochem.,* vol. 38, pp. 889-895, 2000.

[11] R. Peterson and D. Aylor, "Chlorophyll Fluorescence lnduction in Leaves of Phaseolus vulgaris Infected with Bean Rust (Uromycesappendiculatus)," *Plant Physiol,* vol. 108, pp. 163-171, 1995.

[12] A. Porcar-Castell, E. Tyystjarvi, J. Atherton, J. van der Tol, J. Flexas, E. Pfundel, J. Moreno, C. Frankenberg and J. Berry, "Linking chlorophyll a fluorescence to photosynthesis for remote sensing applications: mechanisms and challenges," *Journal of Experimental Botany,* vol. 65, pp. 4065-4095, 2014.

[13] D. Cremers and L. Radziemski, Handbook of Laser-Induced Breakdown Spectroscopy, West Sussex,: John Wiley & Sons Ltd., 2006.

[14] R. Kanawade, F. Mahari, C. Klampfl, M. Rhode, C. Knipfer, K. Tangermann-Gerk, W. Adler, M. Schmidt and F. Stelzle, "Qualitative tissue differentiation by analysing the intensity ratios of atomic emission lines using laser induced breakdown spectroscopy (LIBS): prospects for a feedback mechanism for surgical laser systems," *J. Biophotonics,* vol. 8, pp. 153-161, 2015.

[15] D. Marcos-Martinez, J. Ayala, R. Izquierdo-Hornillos, F. Manuel de Villena and J. Caceres, "“Identification and discrimination of bacterial strains by laser induced breakdown spectroscopy and neural networks," *Talanta,* vol. 84, pp. 730-737, 2011.

[16] A. Samuels, F. DeLucia Jr., K. McNesby and A. Miziolek, "Laser-induced breakdown spectroscopy of bacterial spores, molds, pollens, and protein: initial studies of discrimination potential," *Applied Optics,* vol. 42, pp. 6205-6209, 2003.

[17] B. Bousquet, G. Travalle, A. Ismael, L. Canioni, K. Michel-Le Pierres, E. Brasseur, S. Roy, I. Le Hecho, M. Larregieu, S. Tellier, M. Potin-Gautier, T. Boriachon, P. Wazen, A. Diard and S. Belbeze, "Development of a mobile system based on laser-induced breakdown spectroscopy and dedicated to in situ analysis of polluted soils," *Spectrochimica Acta Part B,* vol. 63, pp. 1085-1090, 2008.

[18] D. Diaz, D. Hahn and A. Molina, "Evaluation of Laser-Induced Breakdown Spectroscopy (LIBS) as a Measurement Technique for Evaluation of Total Elemental Concentration in Soils," *Applied Spectroscopy,* vol. 66, pp. 99-106, 2012.

[19] O. Samek, J. Lambert, R. Hergenroder, M. Liska, J. Kaiser, K. Novotny and S. Kukhlecsky, "Femtosecond laser spectrochemical analysis of plant samples," *Laser Phys. Lett.,* vol. 3, pp. 21-25, 2006.

[20] D. Sun, S. Maugen, C. Dong and X. Ma, "A semi-quantitative analysis of essential micronutrient in folium lycii using laser-induced breakdown spectroscopy technique," *Plasma Science and Technology,* vol. 12, p. 478, 2010.

[21] D. Santos Jr., L. Nunes, G. Carvalho and F. Krug, "Laser-induced breakdown spectroscopy for analysis of plant materials: a review," *Spectrochimica Acta B,* vol. 71, p. 3, 2012.

[22] J. Kaiser, K. Novotny, M. Martin, A. Hrdlicka, R. Malina, M. Hartl, V. Adam and R. Kizek, "Trace elemental analysis by laser-induced breakdown spectroscopy – biological applications," *Surface Science Reports,* vol. 67, p. 233, 2012.

[23] K. Devey, M. Mucalo, G. Rajendram and J. Lane, "Pasture vegetation elemental analysis by laser-induced breakdown spectroscopy," *Communications in Soil Science and Plant Analysis,* vol. 46, p. 72, 2015.

[24] L. Wiles, J. Wilkerson and H. Gold, "Value of information about weed distribution for improving postemergence control decisions," *Crop Prot.,* vol. 11, pp. 547-554, 1992.

[25] J. Norsworthy, S. Ward, D. Shaw, R. Llewellyn, R. Nichols, T. Webster, K. Bradley, G. Frisvold, S. Powles, N. Burgos, W. Witt and M. Barrett, "Reducing the Risks of Herbicide Resistance: Best Management Practices and Recommendations," *Weed Science,* no. Special Issue, pp. 31-62, 2012.

[26] N. A. S. S. o. t. United, *Agricultural Chemical Use Program,* 2014.

[27] D. L. J. J. Martin and Y. Lan, "Laboratory evaluation of the GreenSeeker™ handheld optical sensor to variations in orientation and height above canopy," *Int J Agric & Biol Eng,* vol. 5, pp. 43-47, 2012.

[28] O. Walsh, A. Klatt, J. Solie, C. Godsey and W. Raun, "Use of soil moisture data for refined Greenseeker sensor based nitrogen recommendations in winter wheat (Triticum aestivum L.)," *Precision Agriculture,* vol. 14, p. 343–356, 2013.

[29] E. Lehoczky, J. Tamas, P. Riczu and M. Herdon, "Weed mapping based on integrated remote," in *Proceedings in World Conference on Computers in Agriculture and Natural*, San Jose, Costa Rica, 2014.

[30] U. Weiss, P. Biber, S. Laible, K. Bohlmann and A. Zell, "Plant species classification using a 3d," in *Proceedings in Machine Learning and Applications (ICMLA), 2010 Ninth International Conference*, Washington D.C., 2010.

[31] D. Andujar, M. Weis and R. Gerhards, "An Ultrasonic System for Weed Detection in Cereal Crops," *Sensors,* vol. 12, pp. 17343-17357, 2012.

[32] Q. Zaman, T. Esau, A. Schumann, D. Percival, Y. Chang, S. Read and A. Farooque, "Development of prototype automated variable rate sprayer for real-time spot-application of agrochemicals in wild blueberry fields," *Computers and Electronics in Agriculture,* vol. 76, pp. 175-182, 2011.

[33] W. Nijland, R. de Jong, S. de Jong, M. Wulder, C. Bater and N. Coops, "Monitoring plant condition and phenology using infrared sensitive consumer grade digital cameras," *Agricultural and Forest Meteorology,* vol. 184, pp. 98-106, 2014.

[34] R. Gerhards and S. Christensen, "Real-time weed detection, decision making and patch spraying in maize, sugarbeet, winter wheat and winter barley," *Weed Research,* vol. 43, pp. 385-392, 2003.

[35] D. Lamb, M. Weedon and L. Rew, "Evaluating the accuracy of mapping weeds in seedling crops using airborne digital imaging: Avena spp. in seedling triticale," *Weed Research,* vol. 39, pp. 481-492, 1999.

[36] E. Hestir, S. Khanna, M. Andrew, M. Santos, J. Viers, J. Greenberg, S. Rajapakse and S. Ustin, "Identification of invasive vegetation using hyperspectral remote sensing in the California Delta ecosystem," *Remote Sensing of Environment,* vol. 112, pp. 4034-4047, 2008.

[37] P. Goel, S. Prasher, J. Landry, R. Patel, R. Bonnell, A. Viau and J. Miller, "Potential of airborne hyperspectral remote sensing to detect nitrogen deficiency and weed infestation in corn," *Computers and Electronics in Agriculture,* vol. 38, pp. 99-124, 2003.

[38] J. Singh and S. Thakur, Laser-Induced Breakdown Spectroscopy, Amsterdam: Elsevier, 2007.

[39] A. Miziolek, V. Palleschi and I. Schechter, Laser-Induced Breakdown Spectroscopy (LIBS): Fundamentals and Applications, Cambridge: University Press, 2006.

[40] G. Gamble, B. Park, S. Yoon and K. Lawrence, "Effect of Sample Preparation on the Discrimination of Bacterial Isolates Cultured in Liquid Nutrient Media Using Laser-Induced Breakdown Spectroscopy (LIBS)," *Applied Spectroscopy,* vol. 70, pp. 494-504, 2016.

[41] R. Gaudiuso, M. Dell' Aglio, O. De Pascale, G. Senesi and A. De Giacomo, "Laser Induced Breakdown Spectroscopy for Elemental Analysis in Environmental, Cultural Heritage and Space Applications: A Review of Methods and Results," *Sensors,* vol. 10, pp. 7434-7468, 2010.

[42] J. Wang, P. Zheng, H. Liu and L. Fang, "Classification of Chinese tea leaves using laser-induced breakdown spectroscopy combined with the discriminant analysis method," *Anal. Methods,* vol. 8, pp. 3204-3209, 2016.

[43] M. Andersen, J. Frydenvang, P. Henckel and A. Rinnan, "The potential of laser-induced breakdown spectroscopy for industrial at-line monitoring of calcium content in comminuted poultry meat," *Food Control,* vol. 64, pp. 226-233, 2016.

[44] D. Tripathi, V. Singh, S. Prasad, N. Dubey, D. Chauhan and A. Rai, "LIB spectroscopic and biochemical analysis to characterize lead toxicity alleviative nature of silicon in wheat (Triticum aestivum L.) seedlings," *Journal of Photochemistry & Photobiology, B,* vol. 154, pp. 89-98, 2016.

[45] G. Bilge, I. Boyaci, K. Eseller, U. Tamer and S. Cakir, "Analysis of bakery products by laser-induced breakdown spectroscopy," *Food Chemistry,* vol. 181, pp. 186-190, 2015.

[46] G. Kim, J. Kwak, J. Choi and K. Park, "Detection of Nutrient Elements and Contamination by Pesticides in Spinach and Rice Samples Using Laser-Induced Breakdown Spectroscopy (LIBS)," *J. Agric. Food Chem.,* vol. 60, pp. 718-724, 2012.

[47] G. Carvalho, J. Moros, D. Santos, F. Krug and J. Laserna, "Direct determination of the nutrient profile in plant materials by femtosecond laser-induced breakdown spectroscopy," *Analytica Chemica Acta.,* vol. 876, pp. 26-38, 2015.

[48] D. J. Santos, L. Nunes, G. Carvalho, M. Silva Gomes, P. Souza, F. Oliveira Leme, L. Santos and F. Krug, "Laser-induced breakdown spectroscopy for analysis of plant materials: A review," *Spectrochimica Acta Part B.,* Vols. 71-72, pp. 3-13, 2012.

[49] H. Chen, H. Li, Y. Sun, Y. Wang and P. Lu, "Femtosecond laser for cavity preparation in enamel and dentin: ablation efficiency related factors," *Scientific Reports,* vol. 6, pp. 1-8, 2016.

[50] Z. Dong, X. Zhou, J. Wu, Z. Zhang, T. Li, Z. Zhou, S. Zhang and G. Li, "Small incision lenticule extraction (SMILE) and femtosecond laser LASIK: comparison of corneal wound healing and inflammation," *Br J Ophthalmol,* vol. 0, pp. 1-7, 2013.

[51] A. Farjo, A. Sugar, S. Schallhorn, P. Majmudar, D. Tanzer, W. Trattler, J. Cason, K. Donaldson and G. Kymionis, "Femtosecond Lasers for LASIK Flap Creation," *Ophthalmology,* vol. 120, pp. e5-e20, 2013.

[52] F. Chen and J. Vasquez de Aldana, "Optical waveguides in crystalline dielectric materials produced by femtosecond-laser micromachining," *Laser Photonics Rev.,* vol. 8, pp. 251-275, 2014.

[53] K. Knudsen, "Carbohydrate and lignin contents of plant materials used in animal feeding," *Animal Feed Science and Technology,* vol. 67, pp. 319-338, 1997.

[54] W. Herman, W. McGill and J. Dormaar, "Effects of initial chemical composition on decomposition of roots of three grass species," *Canadian Journal of Soil Sciences,* vol. 57, pp. 205-215, 1977.

[55] S. Zhang, X. Wang, M. He, Y. Jiang, B. Zhang, W. Hang and B. Huang, "Laser-induced plasma temperature," *Spectrochemica Acta Part B,* vol. 97, pp. 13-33, 2014.

[56] C. U.S. Department of Health and Human Services, "Antibiotic Resistance Threats in the United States," 2013.

[57] J. Chen, T. Cesario and P. Rentzepis, "Rationale and mechanism for the low photoinactivation rate of bacteria in plasma," *PNAS,* vol. 111, pp. 33-38, 2014.

[58] F. Vantansever, W. Melo, P. Avci, D. Vecchio, M. Sadasivam, A. Gupta, R. Chandran, M. Karimi, N. Parizotto, R. Yim, G. Tegos and M. Hamblin, "Antimicrobial strategies centered around reactive oxygen species-bacterial antibiotics, photodynamic therapy, and beyond," *FEMS Microbial Rev.,* vol. 37, pp. 955-989, 2013.

[59] J. Wu, H. Xu, W. Tang, R. Kopelman, M. Philbert and C. Xi, "Eradication of bacteria in suspension and biofilms using methylene blue-loaded dynamic nanoplatforms," *Antimicrob. Agents Chemother.,* vol. 53, pp. 3042-3048, 2009.

[60] T. Simon, S. Boca-Farcau, A. Gabudean, P. Baldeck and S. Astilean, "LED-activated methylene blue-loaded Pluronic-nanogold hybrids for in vitro photodynamic therapy," *J. Biophotonics,* vol. 6, pp. 950-959, 2013.

[61] V. Zharov, K. Mercer, E. Galitovskaya and M. Smeltzer, "Photothermal Nanotherapeutics and Nanodiagnostics for Selective Killing of Bacteria Targeted with Gold Nanoparticles," *Biophysical Journal,* vol. 90, p. 619–627, 2006.

[62] G. Santos, F. de Santi Ferrara, F. Zhao, D. Rodrigues and W. Shih, "Photothermal inactivation of heat-resistant bacteria on nanoporous gold disk arrays," *OPTICAL MATERIALS EXPRESS,* vol. 6, pp. 1217-1229, 2016.

[63] T. Dai, A. Gupta, Y. Huang, R. Yin, C. Murray, M. Vrahas, M. Sherwood, G. Tegos and M. Hamblin, "Blue Light Rescues Mice from Potentially Fatal Pseudomonas aeruginosa Burn Infection: Efficacy, Safety, and Mechanism of Action," *Antimicrob. Agents Chemother.,* vol. 57, p. 1238–1245, 2013.

[64] A. Gupta, P. Avci, T. Dai, Y. Huang and M. Hamblin, "Ultraviolet radiation in wound care: sterilization and stimulation," *Advances in Wound Care,* vol. 2, pp. 422-437, 2012.

[65] C. Meulemans, "The basic principles of UV-disinfection of water," *Ozone: Science & Engineering,* vol. 9, pp. 299-313, 1986.

[66] R. Wolfe, "Ultraviolet disinfection of potable water," *Environ. Sci. Technol.,* vol. 24, pp. 768-773, 1990.

[67] G. Ko, M. First and H. Burge, "The characterization of upper-room ultraviolet germicidal irradiation in inactivating airborne microorganisms," *Environmental Health Perspectives,* vol. 110, pp. 95-101, 2002.

[68] N. Reed, "The history of Ultraviolet germicidal irradiation for air disinfection," *Public Health Reports,* vol. 125, pp. 15-27, 2010.

[69] W. Kowalski, W. Bahnfleth, D. Witham, B. Severin and T. Whittam, "Mathematical modeling of Ultraviolet germicidal irradiation for air disinfection," *Quantitative Microbiology,* vol. 2, p. 249–270, 2000.

[70] J. Chang, S. Ossoff, D. Lobe, M. Dorman, C. Dumais, R. Qualls and J. Johnson, "UV inactivation of pathogenic and indicator microorganisms," *APPLIED AND ENVIRONMENTAL MICROBIOLOGY,* vol. 49, pp. 1361-1365, 1985.

[71] B. Madge and J. Jensen, "Ultraviolet disinfection of fecal coliform in municipal wastewater: effects of particle size," *Water Environment Research,* vol. 78, pp. 294-304, 2004.

[72] T. Hussain and M. Gondal, "Laser induced breakdown spectroscopy (LIBS) as a rapid tool for material analysis," *Journal of Physics: Conference Series,* vol. 439, p. 012050, 2013.

[73] K. Stelmaszczyk, P. Rohwetter, G. Méjean, J. Yu, E. Salmon, J. Kasparian, R. Ackermann, J. Wolf and L. and Woste, "Long-distance remote laser-induced breakdown spectroscopy using filamentation in air," *APPLIED PHYSICS LETTERS,* vol. 85, pp. 3977-3979, 2004.

[74] F. Capitelli, F. Colao, M. Provenzano and R. Fantoni, "Determination of heavy metals in soils by Laser Induced Breakdown Spectroscopy," *Geoderma,* vol. 106, p. 45–62, 2002.

[75] X. Fang and S. Ahmad, "Elemental analysis in environmental land samples by stand-off laser-induced breakdown spectroscopy," *Appl. Phys. B,* vol. 115, p. 497–503, 2014.

[76] L. Trevizan, D. Santos Jr., R. Samad, N. Vieira Jr., L. Nunes, I. Rufini and F. Krug, "Evaluation of laser induced breakdown spectroscopy for the determination of micronutrients in plant materials," *Spectrochimica Acta Part B,* vol. 64, p. 369–377, 2009.

[77] M. Bossu, H. Zuo-Qiang, M. Baudelet, Y. Jin, Z. Zhe and Z. Jie, "Femtosecond Laser-Induced Breakdown Spectroscopy for Detection of Trace Elements in Sophora Leaves," *CHIN.PHYS.LETT.,* vol. 24, p. 3466, 2007.

[78] A. Assion, M. Wollenhaupt, L. Haag, F. Mayorov, C. Sarpe-Tudoran, M. Winter, U. Kutschera and T. Baumert, "Femtosecond laser-induced-breakdown," *Appl. Phys. B,* vol. 77, p. 391–397, 2003.

[79] M. Galiová, J. Kaiser, K. Novotný, O. Samek, L. Reale, R. Malina, K. Páleníková, M. Liška, V. Čudek, V. Kanický, V. Otruba, A. Poma and A. Tucci, "Utilization of laser induced breakdown spectroscopy for investigation of the metal accumulation in vegetal tissues," *Spectrochimica Acta Part B,* vol. 62, p. 1597–1605, 2007.

[80] A. Kumar, F. Yueh, J. Singh and S. Burgess, "Characterization of malignant tissue cells by laser-induced breakdown spectroscopy," *APPLIED OPTICS,* vol. 43, pp. 5399-5403, 2004.

[81] M. Baudelet, L. Guyon, J. Yu, J. Wolf, T. Amodeo, E. Fréjafon and P. Laloi, "Femtosecond time-resolved laser-induced breakdown spectroscopy for detection and identification of bacteria: A comparison to the nanosecond regime," *JOURNAL OF APPLIED PHYSICS,* vol. 99, p. 084701, 2006.

[82] G. M´ejean, J. Kasparian, J. Yu, S. Frey, E. Salmon and J. Wolf, "Remote detection and identification of biological aerosols using a femtosecond terawatt lidar system," *Appl. Phys. B,* vol. 78, p. 535–537, 2004.

[83] G. Carter, "Responses of leaf spectral reflectanc to plant stress," *American Journal of Botany,* vol. 80, pp. 239-243, 1993.

[84] T. Simon, S. Boca-Farcau, A. Gabudean, P. Baldeck and S. Astilean, "LED-activated methylene blue-loaded Pluronic-nanogold hybrids for in vitro photodynamic therapy," *J. Biophotonics,* vol. 6, p. 950–959, 2013.

[85] N. Idris, M. Gnanasammandhan, J. Zhang, P. Ho, R. Mahendran and Y. Zhang, "In vivo photodynamic therapy using upconversion nanoparticles as remote-controlled nanotransducers," *Nature Medicine,* vol. 18, pp. 1580-1586, 2012.

[86] S. Bhana, R. O'Connor, J. Johnson, J. Ziebarth, L. Henderson and X. Huang, "Photosensitizer-loaded gold nanorods for near infrared photodynamic and photothermal cancer therapy," *Journal of Colloid and Interface Science,* vol. 469, pp. 8-16, 2016.

[87] C. Ayala-Orozco, C. Urban, M. Knight, A. Urban, O. Neumann, S. Bishnoi, S. Mukherjee, A. Goodman, H. Charron, T. Mitchell, M. Shea, R. Roy, S. Nanda, R. Schiff, N. Halas and A. Joshi, "Au Nanomatryoshkas as Efficient Near-Infrared Photothermal Transducers for Cancer Treatment: Benchmarking against Nanoshells," *ACS Nano,* vol. 8, p. 6372–6381, 2014.

[88] M. El-Azizi and N. Khardori, "Efficacy of ultraviolet C light at sublethal dose in combination with antistaphylococcal antibiotics to disinfect catheter biofilms of methicillin-susceptible and methicillin-resistant Staphylococcus aureus and Staphylococcus epidermidis in vitro," *Infection and Drug Resistance,* vol. 9, p. 181–189, 2016.

[89] S. Dean, A. Petty, S. Swift, J. McGhee, A. Sharma, S. Shah and J. Craig, "Efficacy and safety assessment of a novel ultraviolet C device for treating corneal bacterial infections," *Clinical and Experimental Ophthalmology,* vol. 39, p. 156–163, 2011.

[90] H. Lichtenthalerm, "Vegetation stress: an introduction to the stress concept in plants," *J. Plant Physiol,* vol. 148, pp. 4-14, 1995.

[91] L. Wiles, H. Gold and G. Wilkerson, "Modeling the uncertainty of weed density estimates to improve post-emergence herbicide control decisions," *Weed Research,* vol. 33, pp. 241-252, 1993.

[92] T. Flowers and A. Yeo, "Ion relations in plants under drought and salinity," *Aust. J. Plant Physiol.,* vol. 13, p. 75, 1986.

[93] I. Slama, T. Ghnaya, A. Savoure and C. Abdelly, "Combined effects of long-term salinity and soil drying on growth water relations, nutrient status and proline accumulation," *C R Biol.,* vol. 331, p. 442, 2008.

[94] J. Martinez, J. Ledent, M. Bajji, J. Kinet and S. Lutts, "Effect of water stress on growth, Na+ and K+ accumulation and water use efficiency," *Plant Growth Regulation,* vol. 41, p. 63, 2003.

[95] J. Pardo and F. Quintero, "Plants and sodium ions: keeping company with the enemy," *Genome Biology,* vol. 3, p. 1017, 2002.

[96] I. Ahmed, F. Cao, M. Zhang, X. Chen, G. Zhang and F. Wu, "Difference in yield and physiological features in response to drought and salinity," *PLOS One,* vol. 8, p. e77869, 2013.

[97] H. Knight, A. Trewavas and M. Knight, "Calcium signalling in Arabidopsis thaliana responding to drought and salinity," *Plant J.,* vol. 12, p. 1067, 1997.

[98] A. Price and G. Hendry, "Iron-catalysed oxygen radical formation and its possible contribution to drought damage in nine native grasses and three cereals," *Plant, Cell and Environment,* vol. 14, pp. 477-484, 1991.

[99] G. Mejean, J. Kasparian, J. Yu, S. Frey, E. Salmon and J. Wolf, "Remote detection and identification of biological aerosols using a femtosecond terawatt lidar system," *Appl. Phys. B,* vol. 78, pp. 535-537, 2004.

[100] L. Eleuch, A. Jilal, S. Grando, S. Ceccarelli, M. Schmising, H. Tsujimoto, A. Hajer, A. Daaloul and M. Baum, "Genetic diversity and association analysis for salinity tolerance," *J. Integ. Plant Biol.,* vol. 50, p. 1004, 2008.

[101] F. Fortes and J. Laserna, "The development of fieldable laser-induced breakdown spectrometer: No limits on the horizon," *Spectrochimica Acta Part B,* vol. 65, p. 975–990, 2010.

[102] M. El-Azizi and N. Khardori, "Efficacy of ultraviolet C light at sublethal dose in combination with antistaphylococcal antibiotics to disinfect catheter biofilms of methicillin-susceptible and methicillin-resistant Staphylococcus aureus and Staphylococcus epidermis in vitro," *Infection and Drug Resistance,* vol. 9, pp. 181-189, 2016.

[103] J. Castillo-Martinez, G. Martinez-Castanon, F. Martinez-Gutierrez, N. Zavala-Alonso, N. Patino-Marin, N. Nino-Martinez, V. Zaragoza-Magana and C. Cabral-Romero, "Antibacterial and antibiofilm activities of the photothermal therapy using gold nanorods against seven different bacterial strains," *Journal of Nanomaterials,* vol. 2015, pp. 1-7, 2015.

[104] L. Austin, M. Mackey, E. Dreaden and M. El-Sayed, "The optical, photothermal, and facile surface chemical properties of gold and silver nanoparticles in biodiagnostics, therapy, and drug delivery," *Arch. Toxicol.,* vol. 88, pp. 1391-1417, 2014.

[105] S. Perni, C. Piccirillo, A. Kafizas, M. Uppal, J. Prattan, M. Wilson and I. Parkin, "Antibacterial activity of light-activated silicone containing methylene blue and gold nanoparticles of different sizes," *J. Clust. Sci.,* vol. 21, pp. 427-438, 2010.

[106] B. Pidhatika, J. Moller, E. Benetti, R. Konradi, E. Rakhmatullina, A. Muhlebach, R. Zimmermann, C. Werner, V. Vogel and M. Textor, "The role of the interplay between polymer architecture and bacterial surface properties on microbial adhesion to polyazoline-based thin films," *Biomaterials,* vol. 31, pp. 9462-9472, 2010.

[107] L. Liu, K. Xu, H. Wang, J. Tan, W. Fan, S. Venkatraman, L. Li and Y. Yang, "Self-assembled cationic peptide nanoparticles as an efficient antimicrobial agent," *Nature Nanotechnology,* vol. 4, pp. 457-463, 2009.

[108] E. Hall and A. Giaccia, Radiobiology for the Radiologist, Philidelphia, PA: Lippincott Williams & Wilkins, 2006.

[109] B. Madge and J. Jensen, "Ultraviolet disinfection offFecal coliform in municipal wastewater: effects of particle size," *Water Environment Research,* vol. 78, pp. 294-304, 2006.